52 4-25-95 JS (2)

ANL-95/6

Energy Technology Division
Energy Technology Division
Energy Technology Division
Energy Technology Division
Energy Technology Division
Energy Technology Division
Energy Technology Division
Energy Technology Division
Energy Technology Division
Energy Technology Division
Energy Technology Division
Energy Technology Division
Energy Technology Division
Energy Technology Division
Energy Technology Division
Energy Technology Division
Energy Technology Division
Energy Technology Division
Energy Technology Division
Energy Technology Division
Energy Technology Division
Energy Technology Division
Energy Technology Division
Energy Technology Division
Energy Technology Division
Energy Technology Division
Energy Technology Division
Energy Technology Division
Energy Technology Division
Energy Technology Division
Energy Technology Division
Energy Technology Division
Energy Technology Division
Energy Technology Division

First Assessment of Computations of Turbulent Bubbly Flow and Particulate Flow with the COMMIX-M Program

by M. Bottoni, F. C. Chang, and J. Ding

Argonne National Laboratory, Argonne, Illinois 60439
operated by The University of Chicago
for the United States Department of Energy under Contract W-31-109-Eng-38

Energy Technology Division
Energy Technology Division
Energy Technology Division
Energy Technology Division
Energy Technology Division
Energy Technology Division
Energy Technology Division
Energy Technology Division

Reproduced from the best available copy.

Available to DOE and DOE contractors from the
Office of Scientific and Technical Information
P.O. Box 62
Oak Ridge, TN 37831
Prices available from (615) 576-8401

Available to the public from the
National Technical Information Service
U.S. Department of Commerce
5285 Port Royal Road
Springfield, VA 22161

Distribution
Category:
Advanced Coal Research
UC-113

ARGONNE NATIONAL LABORATORY
9700 South Cass Avenue, Argonne, Illinois 60439

ANL-95/6

FIRST ASSESSMENT OF COMPUTATIONS OF TURBULENT BUBBLY FLOW AND PARTICULATE FLOW WITH THE COMMIX–M PROGRAM

by

M. Bottoni, F. C. Chang, and J. Ding

Energy Technology Division

May 1994

Work sponsored by

U.S. Department of Energy
Pittsburgh Energy Technology Center
Advanced Power Generation Fundamental Research Division

Contents

Figures

Tables

Nomenclature

A_C Acceleration modulus, defined by Eq. 4.3.6

A_i Interfacial area per unit volume (m^2/m^3)

A Cross flow area (m^2)

A_n Amplitude in velocity spectrum of fluid (m)

a_n Amplitude in velocity spectrum of particles (m)

c_1 Constant (= 2.8), used in Eq. 3.2.1.13

c_2 Constant (= 0.47), used in Eq. 3.2.1.13

c_3 Constant (= 0.47), used in Eq. 3.2.1.13

$c_{1\varepsilon}$ Constant (= 1.44), used in Eq. 3.2.1.2

$c_{2\varepsilon}$ Constant (= 1.92), used in Eq. 3.2.1.2

$c_{3\varepsilon}$ Constant (= 0.8), used in Eq. 3.2.1.2

$c_{1\phi}$ Constant (= 3.1), used in Eq. 3.2.1.11

$c'_{1\phi}$ Constant (= 0.5), used in Eq. 3.2.1.11

$c_{2\phi}$ Constant (= 0.5), used in Eq. 3.2.1.11

$c_{3\phi}$ Constant (= 0.5), used in Eq. 3.2.1.11

C_D Friction coefficient

c_k Constant (= 0.09), used in Eq. 3.2.1.13

c_p Specific heat (J/kg–K)

$c_{s\phi}$ Constant (= 0.07), used in Eq. 3.2.1.8

C_{vm} Virtual mass coefficient

c_μ Constant (= 0.09), used in Eq. 3.2.1.14

$c_{\pi k}$ Constant (= 0.02), used in Eq. 3.2.2.4

$c_{\pi\varepsilon}$ Constant (= 1.2), used in Eq. 3.2.2.6

c'_ϕ Constant (= 0.13), used in Eq. 3.2.1.12

$D(v)$ Dissipation spectrum of turbulent kinetic energy (m^3/s^3)

d_b Particle diameter (m)

E Constant (= 9.0), used in Eq. 3.2.1.16

$\vec{F}_L$ Lift force per unit volume (N/m^3)

$\vec{F}_{vm}$ Virtual mass force per unit volume (N/m^3)

$\vec{f}_{vm}$ Virtual mass force acting on one particle (N)

G Production or suppression of turbulence kinetic energy due to buoyancy ($J/s\text{-}m^3$)/mass flow (kg/s)

$G_{i\phi}$ Buoyancy production in scalar flux equations ($m\text{-}K/s^2$)

g $\left(= \frac{1}{2}\overline{\phi^2}\right)$, one-half of the variance of temperature fluctuations (K^2)

$\vec{g}$ Gravity acceleration (m/s^2)

g_i Components of gravitational acceleration (i = 1, 2, and 3) (m/s^2)

H Attenuation of turbulent kinetic energy due to particles

h Specific enthalpy (J/kg)

K Turbulence kinetic energy (J/kg)

K_{ij}^M Drag force between components i and j (kg/m^3s)

Ku Kurtosis

L Length scale (m)

L Force (N)

m_b Mass of a particle (kg)

n (= N/V_f) Number density of particles in a computational cell (m^{-3})/frequency (s^{-1})

N Number of particles in a cell of volume V_f

P Mean shear production in k and ε equations ($J/s\text{-}m^3$)

$P_{i\phi}$ Mean field production in scalar flux equations (i = 1, 2, and 3) ($m\text{-}K/s^2$)

p Pressure (N/m^2)

$\mathcal{Q}$ Specific power generation (W/m^3)/volumetric flow (m^3/h)

q Heat flux (W/m^2)

r Particle or bubble radius (m)

r Coordinate direction (m)

R Constant (= 0.5), used in Eq. 3.2.1.12

Re Reynolds number

R_f (= – G/P), flux Richardson number

R_m Normalized root mean squared relative velocity between the phases

S Skewness

$\bar{\bar{S}}$ Strain rate term, defined by Eq. 4.1.4

T Temperature (K)

T* Temperature, defined by Eq. 3.2.1.23 (K)

T(v) Energy flux (m^2/s^3)

t Time (s)

U_i Components of mean velocity (i = 1, 2, and 3) (m/s)

u_i Fluctuation of velocity component (i = 1, 2, and 3) (m/s)

u_n Fluctuation of velocity component normal to the wall (m/s)

u^* Friction velocity (m/s)

$\bar{U}$ Mean flow velocity (m/s)

u Fluctuation of velocity (m/s)

u^+ Dimensionless velocity defined by Eq. 3.2.1.16

$\overline{u\phi}$ (= Φ) scalar heat flux in the x_1 coordinate direction (m–K/s)

$\overline{u_i u_j}$ Reynolds stress (m^2/s^2)

$\bar{V}$ Momentum density source arising from viscous dissipation (Kg/m^2s^2)

V_b Particle volume (m^3)

V_g (= NV_b) Volume of particles in a computational cell (m^3)

V_f Fluid volume in a control cell (m^3)

v Velocity component (m/s)

$\overline{v\phi}$ Scalar heat flux in the x_2 coordinate direction (m-k/s)

W Mass concentration of particles

W_e Weber number

w Velocity component (m/s)

$\overline{w\phi}$ Scalar flux in the x_3 coordinate direction (m-k/s)

x Flowing quality

x_i Coordinate (i = 1, 2, and 3) (m)

x_n Distance from the wall (m)

y Coordinate direction (m)

y_l Thickness of laminar sublayer (m)

y_ℓ^+ Dimensionless thickness of laminar sublayer

y_p Distance of node p from the wall (m)

z Coordinate direction (m)

Greek

α Volume fraction

$\bar{\alpha}$ Constant defined by Eq. 3.2.3.3

α_n Constant defined by Eq. 3.2.3.10

β $\left[= \frac{1}{\rho}\left(\frac{\partial \rho}{\partial T}\right)_p\right]$, volume expansion coefficient at constant pressure (K^{-1})

Γ Mass transfer rate between phases (kg/m^3s)

Γ_g Total (laminar plus turbulent) diffusivity in temperature fluctuation equation (m^2/s)

Γ_{gl} $\left(= \frac{\lambda}{\rho c_p}\right)$, laminar diffusivity ($m^2/s$)

Γ_{gt} $\left(= c'_{\phi}\frac{k^2}{\varepsilon}\right)$, turbulent diffusivity (m^2/s)

Γ_{ϕ} $\left(= \rho\Gamma^{\nu}_{\phi} = \mu_{\ell} + \rho c_{s\phi}\frac{K^2}{\varepsilon}\right)$, total (laminar plus turbulent) dynamic diffusivity in scalar heat flux equations (m^2/s)

Γ^{ν}_{ϕ} $\left(= \nu_{\ell} + c_{s\phi}\frac{K^2}{\varepsilon}\right)$, total (laminar plus turbulent) kinematic diffusivity in scalar heat flux equations (kg/m–s)

γ Constant defined by Eq. 3.2.3.4

δ Constant defined by Eq. 3.2.3.5

δ_n Constant defined by Eq. 3.2.3.11

δ_{ij} Kronecker delta

Δ Divergence of fluid velocity (s^{-1})

ε Dissipation of turbulence kinetic energy (W/kg)

η Reduced viscosity, defined by Eq. 4.2.2.4/Kolmogorov microscale of length (m)

θ Azimuthal coordinate

θ_n Phase lag

λ Thermal conductivity (W/m–K)

λ_n Phase angle in velocity spectrum

μ_l Laminar dynamic viscosity (kg/m–s)

μ_t Turbulent dynamic viscosity (kg/m–s)

ν Wave number (m^{-4})

ν_l Laminar kinematic viscosity (m^2/s)

ν_t Turbulent kinematic viscosity (m^2/s)

ξ Constant (= 1.5) introduced in Eq. 3.2.3.18

Π Production of turbulent kinetic energy due to particles (W/m^3)

$\pi_{i\phi}$ Pressure–scalar gradient correlation in scalar heat flux equations (m–K/s^2)

ρ Density (kg/m^3)

σ Surface tension (N/m^2)/standard deviation

σ^2 Variance

σ_k (= 1.0), turbulence Prandtl number

σ_t (= 0.9), turbulence Prandtl number for heat transport

σ_ε (= 1.3), turbulence Prandtl number for ε

τ Shear stress (N/m^2)

ϕ Temperature fluctuation (K)

$\overline{\phi}^2$ Variance of temperature fluctuations (K^2)

χ (= 0.41) von Karman constant

ω_n Angular velocity in velocity spectrum (s^{-1})

Indices

b Bubble or particle

i Free or dummy index

j Free or dummy index

k Phase or component

g Gas/air

l Laminar/fluid

L Lift

n Normal to the wall

p Particle

P First computational node close to the wall

S_l Slip

TP Two-phase

t	Turbulence
T	Transpose
vm	Virtual mass
w	Wall

First Assessment of Computations of Turbulent Bubbly Flow and Particulate Flow with the COMMIX–M Program

by

M. Bottoni, F. C. Chang, and J. Ding

Abstract

The COMMIX–M computer code, which describes steady–state and transient single– and multicomponent flows in engineering systems, has been implemented to simulate suspension flows in laminar regimes and turbulent and bubbly particulate flows. This report presents a synopsis of the present code's capabilities, with particular emphasis on the recent development of turbulence models, and explains in detail the modifications necessary to simulate particulate flows and bubbly flows. First results of computations of turbulent bubbly and particulate flows are then given and compared with results of computations reported in the literature and with preliminary experimental results obtained at the Kernforschungszentrum Karlsruhe (Germany).

1 Introduction

The COMMIX–M computer code describes steady–state and transient single– and multicomponent flows in complex engineering systems. Recently, the code has been developed to simulate suspension flows in a laminar regime and turbulent bubbly and particulate flows. A two–phase turbulence model has been modified to be applicable to the latter simulations.

The goal of this report is to make a first assessment of the capability of the code to simulate turbulent bubbly and particulate flows.

In Sec. 2 of the report, we present a synopsis of the main code characteristics. The fundamental equations solved, including those for the turbulence models, are presented in Sec. 3. The most important code developments, which have enabled the simulation of suspension and bubbly flows with respect to the computation of lift forces, drag forces, and virtual mass forces, are explained in Sec. 4. Preliminary computation results are presented in Sec. 5 for bubbly flow and in Sec. 6 for particulate flow. These results enable us to identify the deficiencies of the current models, and therefore, provide a hint of how the program must be improved. Processing of output data for computing energy spectral distributions of velocity fluctuations is explained in Sec. 7.

2 Synopsis of COMMIX–M Code

The COMMIX–M code was developed in 1987–1988 by H. M. Domanus, T. H. Chien, and R. C. Schmitt of the Analytical Thermal Hydraulics Section of the Materials and Components Technology (MCT) Division, now reorganized as the Energy Technology (ET) Division of Argonne National Laboratory. Code development resumed in 1990 and is currently carried on by all staff members of the above-mentioned section.

The code describes steady-state and transient thermal and fluid–dynamic problems in multiphase or multicomponent flows in general two– or three–dimensional geometric configurations. The fluid–dynamic problems can be coupled to thermal problems in inner or outer structures.

The program is structured to handle up to 10 different fields (phases or components) even though it has been checked and validated only on the subcase of a limited number of fields, as explained below.

The basic equations for the conservation of mass, momentum, and enthalpy of the components (or phases) are given in Sec. 3. Single–phase flow turbulence can be described on the basis of a K–ε model or of a Reynolds stress model (RSM). This later model is based on six transport equations for the components of the Reynolds stress tensor, on three equations for the transport of turbulent thermal fluxes, and on one equation for the variance of temperature fluctuations. Thus, including the equation for the dissipation of turbulent kinetic energy, 11 equations are used. However, the RSM is still being checked and verified. Simulated two–phase flow turbulence is based on a modified K–ε model, which takes into account the additional production of turbulent kinetic energy due to bubbles. This model is now undergoing verification.

With respect to treatment of the momentum equation, the code consists of two main branches:

1. Only one momentum equation for the mixture is solved; continuity equations are solved for every component separately in terms of mass fractions. In this branch, an enthalpy equation for the mixture can be solved, if required.

2. Separate momentum equations are solved for every component; continuity equations are also solved for every component in terms of volume fractions. No energy equation is used in this branch.

Mass exchange between the phases can be simulated in both branches, but the code does not provide for a boiling model.

Discretization of convective terms in the transport equations is based on first-order upwind discretization or on skew upwinding.[1] The latter scheme is used only for the energy equation. All transport equations are transformed into an algebraic equation that is formally similar to the equation that would be obtained by discretizing a Poisson equation and is simply referred to as a Poisson (–like) equation. The Poisson equation is solved for pressure, enthalpy, and, if required, for turbulent quantities, by using either a direct solver, the Yale Sparse Matrix Package (YSMP)[2] or an iterative method of conjugate gradients.[3] The YSMP technique is applicable to both symmetric and nonsymmetric matrices, whereas the conjugate gradient method assumes that the matrices of coefficients are symmetric and positive definite.

The COMMIX–M code consists of ≈300 subroutines, written in FORTRAN, and ≈50,000 statements. Plotting facilities are available for temperature and velocity distributions, obtained from a restart file. Computer–aided preparation of input data is being linked to the code.

Thus far, the program has been verified in the following cases:

- Laminar flow of immiscible fluids, with different densities and viscosities, between parallel plates. In this case, an analytical solution for the velocity distribution is known. Results of numerical computation agree with analytical results within 1%.[4]

- Analysis of liquid/solid suspensions for which experimental data are available. Results of these simulations have been published.[5]

A single-phase flow version of COMMIX-M is referred to as COMMIX-1C and has been documented in Ref. 6.

3 Fundamental Equations

3.1 Conservation Equations for Mass, Momentum, and Enthalpy

3.1.1 Mass Conservation Equations

The mass conservation equation for every component K is

$$\frac{\partial}{\partial t}(\rho_k \alpha_k) + \nabla \cdot (\rho_k \alpha_k \vec{U}_k) = \Gamma_k, \tag{3.1.1}$$

where $\Gamma_k(kg/m^3s)$ is the mass source.

3.1.2 Momentum Equations

The momentum equation for every component K is

$$\frac{\partial}{\partial t}(\alpha_k \rho_k \vec{U}_k) + \nabla \cdot (\alpha_k \rho_k \vec{U}_k \vec{U}_k) = -\alpha_k \nabla p + \vec{V}_k + \alpha_k \rho_k \vec{g} + K_{kj}^M (\vec{U}_k - \vec{U}_j) + \vec{F}_{Lk} + \vec{F}_{vm,k}, \tag{3.1.2}$$

where $\vec{V}_k$ is the momentum density source arising from viscous dissipation, K_{kj}^M is the drag force at the interface between components k and j, $\vec{F}_L$ is the lift force, and $\vec{F}_{vm}$ is the virtual mass force. The analytical expressions of the latter two forces are given below in apposite sections.

3.1.3 Enthalpy Equations

The enthalpy equation for every component K is

$$\frac{\partial}{\partial t}(\rho_k h_k) + \nabla \cdot (\rho_k h_k \vec{U}_k) = -\nabla \cdot \vec{q}_k + \frac{dp}{dt} + Q_k + \Gamma_k h_k, \tag{3.1.3}$$

where Q_k is the specific power generation. In Eqs. 3.1.2 and 3.1.3, it is assumed that all components have the same pressure.

3.2 Governing Equations for Turbulence Models

3.2.1 Single–Phase Flow

The transport equations for turbulent kinetic energy K and its dissipation ε are

$$\rho\frac{\partial K}{\partial t} + \rho U_j\frac{\partial K}{\partial x_j} = P + G - \rho\varepsilon + \frac{\partial}{\partial x_j}\left[\left(\mu_\ell + \frac{\mu_t}{\sigma_k}\right)\frac{\partial K}{\partial x_j}\right] \tag{3.2.1.1}$$

and

$$\rho\frac{\partial \varepsilon}{\partial t} + \rho U_j\frac{\partial \varepsilon}{\partial x_j} = c_{1\varepsilon}\frac{\varepsilon}{k}(P + G)(1 + c_{3\varepsilon}R_f) - c_{2\varepsilon}\frac{\varepsilon^2}{k} + \frac{\partial}{\partial x_j}\left[\left(\frac{\mu_t}{\sigma_\varepsilon} + \mu_\ell\right)\frac{\partial \varepsilon}{\partial x_j}\right], \tag{3.2.1.2a}$$

or

$$\rho\frac{\partial \varepsilon}{\partial t} + \rho U_j\frac{\partial \varepsilon}{\partial x_j} = c_{1\varepsilon}\frac{\varepsilon}{K}(P + G)(1 + c_{3\varepsilon}R_f) - c_{2\varepsilon}\frac{\varepsilon^2}{K} + \frac{\partial}{\partial x_j}\left(\mu_\ell\frac{\partial \varepsilon}{\partial x_j} + c_\varepsilon\frac{\rho K}{\varepsilon}\overline{u_j u_k}\frac{\partial \varepsilon}{\partial x_k}\right), \tag{3.2.1.2b}$$

with

$$P = \mu_t\left[\frac{\partial U_i}{\partial x_j}\left(\frac{\partial U_i}{\partial x_j} + \frac{\partial U_j}{\partial x_i}\right)\right], \tag{3.2.1.3}$$

$$G = -\rho\beta g_i\overline{u_i\phi}, \tag{3.2.1.4}$$

$$R_f = -\frac{G}{P}, \tag{3.2.1.5}$$

$$\beta = -\frac{1}{\rho}\left(\frac{\partial \rho}{\partial T}\right)_p. \tag{3.2.1.6}$$

Equation 3.2.1.2b, with $c_\varepsilon = 0.15$, is used in combination with Eq. 3.2.1.13 for the Reynolds stress model.

We refer the reader to the Nomenclature list for the definition of the symbols. In the K–ε model, Eq. 3.2.1.4 is approximated by

$$G = -\frac{\mu_t}{\rho\sigma_t}\left(\frac{\partial \rho}{\partial T}\right)_p\left(\frac{\partial T}{\partial x_j}g_j\right). \tag{3.2.1.7}$$

The transport equations for scalar heat fluxes ($\overline{u_i\phi}$: $\overline{u\phi}$, $\overline{v\phi}$, and $\overline{w\phi}$) are

$$\frac{\partial}{\partial t}\left(\overline{u_i\phi}\right) + U_j\frac{\partial}{\partial x_j}\left(\overline{u_i\phi}\right) = \frac{\partial}{\partial x_j}\left[\left(\nu_\ell + c_{s\phi}\frac{K^2}{\varepsilon}\right)\frac{\partial\left(\overline{u_i\phi}\right)}{\partial x_j}\right] + P_{i\phi} + G_{i\phi} + \pi_{i\phi}, \tag{3.2.1.8}$$

with

$$P_{i\phi} = -\left(\overline{u_iu_j}\frac{\partial T}{\partial x_j} + \overline{u_j\phi}\frac{\partial U_i}{\partial x_j}\right), \tag{3.2.1.9}$$

$$G_{i\phi} = -\beta g_i\overline{\phi^2}, \tag{3.2.1.10}$$

and

$$\pi_{i\phi} = -c_{1\phi}\frac{\varepsilon}{K}\overline{u_i\phi} + c_{2\phi}\overline{u_j\phi}\frac{\partial U_i}{\partial x_j} + c_{3\phi}\beta g_i\overline{\phi^2} - c'_{1\phi}\frac{\varepsilon}{K}\overline{u_n\phi}\delta_{in}f\left(\frac{L}{x_n}\right). \tag{3.2.1.11}$$

The transport equation for variance of temperature fluctuations $\left(g = \frac{1}{2}\overline{\phi^2}\right)$ is

$$\frac{\partial g}{\partial t} + \frac{\partial\left(U_j g\right)}{\partial x_j} = \frac{\partial}{\partial x_j}\left[\left(c'_\phi\frac{K^2}{\varepsilon} + \frac{\lambda}{\rho c_p}\right)\frac{\partial g}{\partial x_j}\right] - \overline{u_j\phi}\frac{\partial T}{\partial x_j} - \frac{\varepsilon}{K}\frac{g}{R}. \tag{3.2.1.12}$$

The transport equations for Reynolds stresses $(\overline{u_iu_j})$ are

$$\frac{\partial\left(\overline{u_iu_j}\right)}{\partial t} + U_\ell\frac{\partial\left(\overline{u_iu_j}\right)}{\partial x_\ell} = \frac{\partial}{\partial x_\ell}\left[c_k\frac{K^2}{\varepsilon}\frac{\partial\left(\overline{u_iu_j}\right)}{\partial x_\ell} + \nu_\ell\frac{\partial\left(\overline{u_iu_j}\right)}{\partial x_\ell}\right] - (1 - c_2)\left(\overline{u_iu_\ell}\frac{\partial U_j}{\partial x_\ell} + \overline{u_ju_\ell}\frac{\partial U_i}{\partial x_\ell}\right)$$

$$- \left[\frac{2}{3}\varepsilon\delta_{ij} + c_1\frac{\varepsilon}{K}\left(\overline{u_iu_j} - \frac{2K\delta_{jk}}{3}\right) - \frac{2}{3}c_2\overline{u_nu_m}\frac{\partial u_n}{\partial x_m}\delta_{ij} - (1 - c_3)\beta\left(g_i\overline{u_j\phi} + g_j\overline{u_i\phi}\right)\right]$$

$$+ \frac{2}{3}c_3\beta g_\ell\overline{u_\ell\phi}\,\delta_{ij} - c_1\frac{\varepsilon}{K}\left(\overline{u_iu_j}\right) - (1 - c_3)\beta\left(g_i\overline{u_j\phi} + g_j\overline{u_i\phi}\right). \tag{3.2.1.13}$$

The numerical values of the coefficients used in the above equations are as follows:

$c_{1\varepsilon} = 1.44,$	$c_{2\varepsilon} = 1.92,$	$c_{3\varepsilon} = 0.8,$	$\sigma_k = 1.0,$
$c_{1\phi} = 3.1,$	$c_{2\phi} = 0.4,$	$c_{3\phi} = 0.5,$	$\sigma_t = 0.9,$
$c'_{1\phi} = 0.5,$	$c'_\phi = 0.13,$	$R = 0.5,$	$\sigma_\varepsilon = 1.3,$
$c_1 = 2.8,$	$c_2 = 0.47,$	$c_3 = 0.47,$	$c_{s\phi} = 0.07,$
$c_k = 0.09.$			

The boundary conditions used for the above equation are illustrated in Figs. 1 and 2, which show the two-layer wall function model used in COMMIX-M, where P is the node adjacent to the wall, y_p is the distance from P to the wall, and y_l is the thickness of the viscous sublayer. The distance y_p is fixed, for a given mesh system. The thickness of the viscous sublayer, y_l, however, is not a constant.

When $y_p > y_l$, the first node is in a fully turbulent zone and it holds, for the turbulent kinetic energy and its dissipation,

$$K_p = u^{*2}/\sqrt{c_\mu}, \tag{3.2.1.14}$$

and

$$\varepsilon_p = u^{*3}/(\chi y_p), \tag{3.2.1.15}$$

where

$$u^* = \frac{u_p}{u^+} = \frac{\chi u_p}{\ell n(y + E)}. \tag{3.2.1.16}$$

Equation 3.2.1.16 gives the "universal law of the wall" in terms of friction velocity u*, defined by

$$u^* = \sqrt{\frac{\tau_w}{\rho}}. \tag{3.2.1.17}$$

χ (= 0.42) is the von Karman constant, and E (= 9.0) is a constant that is dependent on the roughness of the wall.

When $y_p < y_l$, the node P is in the laminar sublayer, and one has

$$K_p = u^{*2}(y_p / y_\ell)/\sqrt{c_\mu}, \tag{3.2.1.18}$$

and

$$\varepsilon_p = u^{*3}/(\chi y_\ell). \tag{3.2.1.19}$$

The thickness of the laminar sublayer y_l is evaluated by matching the velocity at the edge of the viscous sublayer ($y = y_l$) to that obtained from the law of the wall. Thus, one has

$$u^+ = y_\ell^+ = \frac{1}{\chi}\ell n(E y_\ell^+), \tag{3.2.1.20}$$

with

$$y_\ell = \nu_\ell y_\ell^+ / u^*. \tag{3.2.1.21}$$

For the scalar fluxes, the boundary conditions are

$$-\left(\overline{u_i\phi}\right)_p = \begin{cases} T^* u^* & \text{if } y_p \geq y_\ell \\ -c_\mu \dfrac{k^2}{\varepsilon} \dfrac{\partial T}{\partial x_i} & \text{if } y_p < y_\ell \end{cases} \tag{3.2.1.22}$$

with

$$T^* = \frac{q_w}{\rho c_p u^*}. \tag{3.2.1.23}$$

The boundary conditions for the variance of the temperature fluctuations are as follows:

If $y_p \geq y_l$,

$$g_p = \frac{T^{*2} R \sigma_t}{\sqrt{c_\mu}}, \tag{3.2.1.24}$$

where σ_t (= 0.9) is the turbulence Prandtl number for heat transport.

If $y_p < y_l$,

$$g_p = \frac{1}{A}\left[\Gamma_{g\ell} \frac{g_\ell}{y_\ell - y_p} + \Gamma_{gp} \frac{g_w}{y_p} + \frac{(u^* T^*)^2 \sigma_t}{2\nu_t} y_\ell - \frac{y_\ell}{R\nu_\ell}(u^* T^*)^2\right], \tag{3.2.1.25}$$

with

$$A = v_p \frac{y_\ell}{y_p} + \frac{\Gamma_{g\ell}}{y_\ell - y_p} + \frac{\Gamma_{gp}}{y_p} \tag{3.2.1.26}$$

and

$$\Gamma_g = c_\phi' \frac{K^2}{\varepsilon} + \frac{\lambda}{\rho c_p}. \tag{3.2.1.27}$$

The boundary conditions for Reynolds stresses are

$$\left(-\overline{u_i u_j}\right)_p = u^{*2} \qquad i \neq j$$

$$\left(\overline{u_i u_j}\right)_p = u^{*2}/\sqrt{c_\mu} \qquad i = j. \tag{3.2.1.28}$$

The above equations, with the relative boundary conditions, can be used in the frame of three different turbulence models at increasing levels of sophistication:

- In the frame of the K–ε model, Eqs. 3.2.1.1 – 3.2.1.7 are used.
- In the frame of a so–called anisotropic turbulence model, Eqs. 3.2.1.1 – 3.2.1.12 are used. Further details about this model are given in Ref. 7.
- In the frame of the Reynolds stress model, Eqs. 3.2.1.2 – 3.2.1.13 are used. In this case, the turbulence kinetic energy is computed as $K = \overline{u_i u_i}/2$.

3.2.2 Multiphase Flow

The K–ε model has been extended to the case of multiphase or multicomponent flows. So far, however, it has been tested and applied only for the case of a two–component flow in which a carrying fluid transports particles.

The transport equation for the turbulence kinetic energy becomes, for every component k:

$$\alpha_k\rho_k \frac{\partial K_k}{\partial t} + \alpha_k\rho_k U_{kj} \frac{\partial K_k}{\partial x_j} = P_k + G_k + \Pi_k - \alpha_k\rho_k\varepsilon_k + \frac{\partial}{\partial x_j}\left[\left(\mu_{\ell k} + \frac{\mu_{tk}}{\sigma_t}\right)\frac{\partial K_k}{\partial x_j}\right], \tag{3.2.2.1}$$

with

$$P_k = \alpha_k\mu_{tk}\frac{\partial U_{ki}}{\partial x_j}\left(\frac{\partial U_{ki}}{\partial x_j} + \frac{\partial U_{kj}}{\partial x_i}\right), \tag{3.2.2.2}$$

$$G_k = \frac{\mu_{tk}}{\rho_k\sigma_t}\frac{\partial(\alpha_k\rho_k)}{\partial T_k}\frac{\partial T_k}{\partial x_j}g_j, \tag{3.2.2.3}$$

and

$$\Pi_k = c_{\pi k}\rho_k(1 - \alpha_k)\frac{\left|\bar{V}_{S\ell}\right|^3}{r_b}. \tag{3.2.2.4}$$

The additional term Π_k, which does not appear in Eq. 3.2.1.1 for single–phase flow, represents the production of turbulent kinetic energy due to particles of radius r_b. V_{Sl} is the slip velocity between carrying fluid and carried particles. We used $c_{\pi k} = 0.02$ in the applications, but the numerical value of this constant is not yet validated.

The transport equation for the dissipation of turbulent kinetic energy becomes

$$\alpha_k\rho_k \frac{\partial \varepsilon_k}{\partial t} + \alpha_k\rho_k U_{kj} \frac{\partial \varepsilon_k}{\partial x_j} = \left[c_{1\varepsilon} \frac{\varepsilon_k}{K_k}(P_k + G_k) + \Pi_{\varepsilon k} \right](1 + c_{3\varepsilon} R_{fk})$$

$$- c_{2\varepsilon}\alpha_k\rho_k \frac{\varepsilon_k^2}{K_k} + \frac{\partial}{\partial x_j}\left[\left(\mu_{\ell k} + \frac{\mu_{tk}}{\sigma_\varepsilon} \right) \frac{\partial \varepsilon_k}{\partial x_j} \right], \qquad (3.2.2.5)$$

where the additional term $\Pi_{\varepsilon k}$, representing the dissipation of turbulent kinetic energy produced by the particles, is given by

$$\Pi_{\varepsilon k} = c_{\pi\varepsilon} \frac{\varepsilon_k}{K_k} \Pi_k, \qquad (3.2.2.6)$$

with $c_{\pi\varepsilon} = 1.2$.

3.2.3 Attenuation of Turbulent Kinetic Energy Due to Small Particles

The additional production of turbulent kinetic energy, modeled by term Π_k in Eq. 3.2.2.1, is due essentially to the formation of a wake beyond the particles and to vortex shedding. The mechanism of vortex shedding is strong at high particle Reynolds numbers,

$$Re_b = \frac{d_b \rho_\ell | \bar{V}_{s\ell} |}{\mu_\ell} \qquad (3.2.3.1)$$

but becomes negligible below $Re_b \approx 400$. At even lower particle Reynolds numbers, for $Re_b < 110$, the turbulent kinetic energy of the carrying fuid is damped because the particles are entrained in the oscillating motion of the fluid turbulent fluctuations and dissipate energy due to shearing. Therefore, when small particles are entrained by a fluid in turbulent motion, the turbulent kinetic energy of the fluid becomes lower than in single-phase flow at the same Reynolds number.

The physical modeling of the attenuation of turbulent kinetic energy due to small particles is summarized in this section, following the treatment of Ref. 8. The implementation of this modeling in the COMMIX-M code is explained at the end of this section.

Let us assume that the particles transported by a fluid are spherical, of uniform size, and have Reynolds number $Re_b < 110$. We further assume that the particle phase is dilute, so that interactions between the particles are negligible. The equation describing the motion of one particle in a turbulent flow is (see, for instance Ref. 9)

$$V_b\rho_b \frac{du_b(t)}{dt} = 6\pi\mu_{\ell t} r_b [u_\ell(t) - u_b(t)] + V_b\rho_\ell \frac{du_\ell(t)}{dt}$$

Term (I) (II) (III)

$$+ C_{vm} V_b \rho_\ell \left[\frac{du_\ell(t)}{dt} - \frac{du_b(t)}{dt}\right] + 6\pi_b^2 \sqrt{\pi \rho_\ell \mu_{\ell t}} \int_o^t \frac{\frac{du_\ell(t')}{dt'} - \frac{du_b(t')}{dt'}}{\sqrt{t - t'}} \qquad (3.2.3.2)$$

(IV) (V)

Eq. 3.2.3.2, originally devised for slow motion of a particle in a stationary fluid, can be applied to turbulent flow by replacing the molecular dynamic viscosity of the fluid μ_ℓ, with the turbulent viscosity, $\mu_{\ell t}$. Terms at the right-hand side of Eq. 3.2.3.2 represent: (II) the viscous force (Stoke's drag force); (III) the force arising from the pressure gradient around the particle, due to fluid acceleration; (IV) the virtual mass force; (V) the transient viscous force or Basset force. Eq. 3.2.3.2 can be rearranged as

$$\frac{du_b(t)}{dt} = \bar{\alpha}\,[u_b(t) - u_\ell(t)] + \gamma \frac{du_\ell(t)}{dt} + \delta \int_o^t \frac{\frac{du_\ell(t')}{dt'} - \frac{du_b(t')}{dt'}}{\sqrt{t - t'}}\,, \qquad (3.2.3.3)$$

with the definition of the coefficients

$$\bar{\alpha} = \frac{18\mu_{\ell t}}{d_b^2(\rho_b + C_{vm}\rho_\ell)}\,, \qquad (3.2.3.4)$$

$$\gamma = \frac{1 + C_{vm}}{\frac{\rho_b}{\rho_\ell} + C_{vm}}\,, \qquad (3.2.3.5)$$

$$\delta = \frac{g\sqrt{\nu_{\ell t}}}{\sqrt{\pi}\, d_b\left(\frac{\rho_b}{\rho_\ell} + C_{vm}\right)}\,. \qquad (3.2.3.6)$$

In Ref. 8, the fluid and particle velocities are decomposed in mean values and turbulent fluctuations, and are represented by their velocity spectra as

$$u_\ell(t) = U_\ell + u_\ell = U_\ell + \sum_1^N{}_n\, u_{\ell n} = U_\ell + \sum_1^N{}_n\, A_n\omega_n \sin(2\pi nt + \lambda_n), \qquad (3.2.3.7)$$

$$u_b(t) = U_b + u_b = U_b + \sum_1^N{}_n\, u_{bn} = U_b + \sum_1^N{}_n\, a_n\omega_n \sin(2\pi nt + \lambda_n - g_n), \qquad (3.2.3.8)$$

where $\omega_n = 2\pi n$ and g_n is the lag in the phase angle between the fluid and particle fluctuations. Introducing Eqs. 3.2.3.7 and 3.2.3.8 into 3.2.3.3 and imposing the condition that for every frequency n, the coefficients multiplying the functions $\sin(\omega_n t + \lambda_n)$ and $\cos(\omega_n t + \lambda_n)$ are equal, one derives an analytical expression for the amplitude ratio, a_n/A_n, and for the phase lag θ_n, as

$$\frac{a_m}{A_m} = \frac{(\alpha_n + \delta_n)^2 + (1 + \delta_n)(\gamma + \delta_n)}{\left[(1 + \delta_n)^2(\gamma + \delta_n)^2\right]\cos\theta_n}\,, \qquad (3.2.3.9)$$

$$tg\theta_n = \frac{(\alpha_n + \delta_n)(1 - \gamma)}{(1 + \delta_n)(\gamma + \delta_n) + (\alpha_n + \delta_n)^2}, \qquad (3.2.3.10)$$

where

$$\alpha_n = \bar{\alpha} / \omega_n, \qquad (3.2.3.11)$$

$$\delta_n = \delta / \sqrt{\pi / 2\omega_n}. \qquad (3.2.3.12)$$

The normalized root-mean-squared (RMS) relative velocity between fluid and particles is obtained as

$$R_n = \frac{(u_{\ell n} - u_{bn})_{RMS}}{(u_{\ell n})_{RMS}} = \left[1 + \left(\frac{a_n}{A_n}\right)^2 - \frac{2a_n}{A_n} \cos\theta_n\right]^{1/2}. \qquad (3.2.3.13)$$

In the subcase in which only viscous forces are important ($\gamma = \delta = o$), one obtains

$$\frac{a_n}{A_n} = \frac{\bar{\alpha}^2}{\left(\omega_n^2 + \bar{\alpha}^2\right) \cos\theta_n}, \qquad (3.2.3.14)$$

$$tg\theta_n = \omega_n / \bar{\alpha}, \qquad (3.2.3.15)$$

while Eq. 3.2.3.13 still holds. This simplifying assumption is used in the numerical application explained in the next section.

Let us define K(ν) and D(ν) as the turbulent kinetic energy and its dissipation per unit wave number ν and

$$W = \frac{\alpha_b \rho_b}{\alpha_b \rho_b + \alpha_\ell \rho_\ell} \qquad (3.2.3.16)$$

the mean concentration of the particles. The dissipation spectrum of the fluid-particles two-phase (TP) flow is then given by

$$D(r)_{TP} = 2\nu_\ell \nu^2 K(\nu)_{TP} + \frac{36\, W \nu_\ell \rho_\ell R_\nu^2}{d_b^2 \rho_b} K(\nu)_{TP}. \qquad (3.2.3.17)$$

The first term at the right-hand side of Eq. 3.2.3.17 is the energy dissipation of the continuous phase, assumed to be formally identical to the dissipation spectrum, $D(\nu) = 2\nu_\ell \nu^2 K(\nu)$, of a single phase flow.[10] The second term is proved in Ref. 8 to represent the energy dissipation arising from the shearing action of the oscillatory motion of the particles entrained by the turbulent oscillations of the fluid. The energy flow through the energy cascade which leads to viscous dissipation of the turbulent kinetic energy in the equilibrium range is given by

$$\frac{dT(\nu)_{TP}}{d\nu} = - D(\nu)_{TP}. \qquad (3.2.3.18)$$

The relationship between the energy flux, T(ν), and the turbulent kinetic energy, K(ν), which has been proven for single-phase flow in the equilibrium range, is assumed to hold also in the two-phase flow case, namely

$$T(\nu)_{TP} = \frac{1}{\xi}\,\varepsilon_{TP}^{1/3}\,\nu^{5/3}\,K(\nu)_{TP}, \tag{3.2.3.19}$$

where $\xi \approx 1.5$ and

$$\varepsilon_{TP} = \int_0^\infty D(\nu)_{TP}d\nu. \tag{3.2.3.20}$$

$$= \int_0^\infty \left(2\nu_\ell \nu^2 + \frac{36\,W\nu_\ell\rho_\ell\,R_\nu^2}{d_b^2\,\rho_b}\right) K(\nu)_{TP}d\nu.$$

(We note that formula 29 of Ref. 8 seems to be wrong. The constant 15 in the first term of the integral should be replaced by 2.)

Combining Eqs. 3.2.3.18 and 3.2.3.19 and integrating, one obtains

$$K(\nu)_{TP} = c\xi\nu^{-5/3}\,\varepsilon_{TP}^{-1/3}\exp\left\{-\frac{3}{2}\,\xi(\eta_{TP}\nu)^{4/3} - \frac{36\,W\rho_\ell\eta_{TP}^{4/3}\xi}{d_b^2\rho_b}\int_o^\nu \nu^{-5/3}\,R_\nu^2 d\nu\right\}, \tag{3.2.3.21}$$

where, in analogy with the definition of Kolmogorov microscale of length in single-phase flow, we use

$$\eta_{TP}^{4/3} = \nu_\ell\varepsilon_{TP}^{-1/3}. \tag{3.2.3.22}$$

The integration constant c in Eq. 3.2.3.21 can be eliminated by imposing the condition that for W = 0 (absence of particles), one obtains the same turbulence spectrum as for single-phase flow, namely[10]

$$K(\nu) = \xi\varepsilon^{2/3}\,\nu^{-5/3}\exp\left\{-\frac{3}{2}\xi(\eta\nu)^{4/3}\right\} \tag{3.2.3.23}$$

Thus, one obtains

$$c\,\varepsilon_{TP}^{-1/3}\exp\left\{-\frac{3}{2}\xi(\eta_{TP}\nu)^{4/3}\right\} = \varepsilon^{2/3}\left\{\exp-\frac{3}{2}\xi(\eta\nu)^{4/3}\right\} \tag{3.2.3.24}$$

and from Eq. 3.2.3.21

$$K(\nu)_{TP} = \xi\varepsilon^{2/3}\,\nu^{-5/3}\exp\left\{-\frac{3}{2}\xi(\eta\nu)^{4/3} - \frac{36W\rho_\ell\xi\eta_{TP}^{4/3}}{d_b^2\,\rho_b}\int_0^\nu \nu^{-5/3}\,R_\nu^2 d\nu\right\} \tag{3.2.3.25}$$

$$= K(\nu) \exp\left\{ - \frac{36 W \rho_\ell \xi \eta_{TP}^{4/3}}{d_b^2 \rho_b} \int_0^\nu \nu^{-5/3} R_\nu^2 d\nu \right\},$$

$$= K(\nu)\, H(\nu),$$

where we defined the attenuation factor

$$H(\nu) = \frac{K(\nu)_{TP}}{K(\nu)} = \exp\left\{ - \frac{36 W \rho_\ell \xi \eta_{TP}^{4/3}}{d_b^2 \rho_b} \int_0^\nu \nu^{-5/3} R_\nu^2 d\nu \right\}. \qquad (3.2.3.26)$$

The main difficulty in applying this theoretical modeling in the COMMIX-M code is that the code computes integral values of the turbulent kinetic energy but not its spectral distribution. Thus, the attenuation factors, which depend on the wave number ν, cannot be used directly. To cope with this difficulty, a spectral distribution must be assumed with the condition that its integration over the full spectrum yields the same turbulent kinetic energy as computed by the code.

Let

$$K_o = \int_o^\infty K(\nu)\, d\nu = \int_o^{\nu_1} K(\nu) d\nu + \int_{\nu_1}^\infty K(\nu) d\nu \qquad (3.2.3.27)$$

be the value computed by the code, for a given computational cell, in a two-phase flow calculation but without accounting for the attenuation of turbulent kinetic energy due to particles. The wave number ν_1 denotes the boundary between the large-scale range and the inertial subrange. In the inertial subrange and in the equilibrium range, the spectral distribution is given by

$$K(\nu) = c_o \nu^{-5/3}. \qquad (3.2.3.28)$$

The proportionality constant c_o must be determined by imposing the condition that the integrated value, according to Eq. 3.2.3.27, is equal to K_o. We impose this condition assuming $\nu_1 \approx 1o^{-1}$ and neglecting the first integral at the right-hand side of Eq. 3.2.3.27. Thus, we obtain

$$c_o \approx \frac{2}{3} K_o \nu_1^{2/3}, \qquad (3.2.3.29)$$

and

$$K(\nu) \approx \frac{2}{3} K_o \nu_1^{2/3} \nu^{-5/3}. \qquad (3.2.3.30)$$

Next, the attenuation factor is computed with Eq. 3.2.3.26 and $K(\nu)_{TP} = K(\nu)\, H(\nu)$ using Eq. 3.2.3.25. Finally, integration of $K(\nu)_{TP}$ yields the updated value

$$K_{\sigma TP} = \int_0^\infty K(\nu)_{TP} d\nu = \int_{\nu_l}^\infty K(\nu) d\nu. \tag{3.2.3.31}$$

The ratio

$$H_\sigma = \frac{K_{\sigma TP}}{K_\sigma} \tag{3.2.3.32}$$

is the integral attenuation of the turbulent kinetic energy due to the particles.

4 Computation of Lift, Drag, and Virtual Mass Forces

The modeling of lift forces is of paramount importance for computing the distribution of volume fractions of the components in suspension flows. Drag forces between the components are important for computing the relative velocities and pressure drops. The stability of the numerical calculations, especially at high Reynolds numbers, is enhanced by the modeling of virtual mass forces. Because these topics are very important for the simulation of suspension and bubbly flows, they are explained in detail in this section. The components of the velocity are not capitalized in this section because there is no ambiguity with turbulent fluctuations.

4.1 Lift Force

A sphere of radius r_b, moving through a viscous liquid with velocity V_{Sl} relative to a uniform simple shear, experiences a lift force

$$L_z = c\,\rho_\ell\, V_{S\ell}\, r_b^2 \left(\nu_\ell \left|\frac{\partial u_\ell}{\partial z}\right|\right)^{1/2} \operatorname{sign}\left(\frac{\partial u_\ell}{\partial z}\right) \text{(N)}, \tag{4.1.1}$$

where ν_l is the kinematic viscosity of the liquid and $\partial u_l/\partial z$ is the velocity gradient perpendicular to the direction of motion. The constant c has been evaluated numerically as $c = 81.2/4\pi \simeq 6.46$.[11] The force L acts in the z direction.

Equation 4.1.1 can be generalized to three coordinate directions with the identity

$$\left|\frac{\partial u_\ell}{\partial z}\right|^{1/2} \operatorname{sign}\left(\frac{\partial u_\ell}{\partial z}\right) = \frac{\dfrac{\partial u_\ell}{\partial z}}{\left|\dfrac{\partial u_\ell}{\partial z}\right|^{1/2}}, \tag{4.1.2}$$

and replacing the velocity gradients with twice the components of the strain rate tensor, which are in Cartesian coordinates;

$$2S_{ij} = 2\left[\frac{1}{2}\left(\frac{\partial u_i}{\partial x_j} + \frac{\partial u_j}{\partial x_i}\right) - \frac{\Delta}{3}\,\delta_{ij}\right]. \tag{4.1.3}$$

In tensor notation, one has

$$2\bar{\bar{S}} = \nabla\bar{u}_\ell + (\nabla\bar{u}_\ell)^T - \frac{2}{3}\Delta\bar{\bar{I}}, \tag{4.1.4}$$

where

$$\Delta = \nabla \bullet \bar{u}_\ell \tag{4.1.5}$$

and the superscript T denotes transpose.

The generalization of Eq. 4.1.2 becomes

$$\frac{2S_{ij}}{(2S_{\ell m}\ S_{m\ell})^{1/4}} = \frac{2S_{ij}}{\left(2\bar{\bar{S}}:\bar{\bar{S}}\right)^{1/4}}, \tag{4.1.6}$$

where S_{lm} is the norm of the matrix formed with the S_{ij} values. Therefore, the generalization of Eq. 4.1.1 can be written

$$L_i = 6.46\rho_\ell\nu_\ell^{1/2} r_b^2 V_{S\ell j} \frac{2S_{ij}}{(2S_{\ell m}\ S_{m\ell})^{1/4}}\ (N) \quad (i = 1, 2, 3 \equiv x, y, z), \tag{4.1.7}$$

or

$$\bar{L} = 6.46\rho_\ell\nu_\ell^{1/2} r_b^2 \bar{V}_{S\ell} \bullet \frac{\left[\nabla\bar{u}_\ell + (\nabla\bar{u}_\ell)^T - \frac{2\Delta}{3}\bar{\bar{I}}\right]}{(2S_{\ell m}\ S_{m\ell})^{1/4}}. \tag{4.1.8}$$

Letting $\bar{u} = (u, v, w)$, the components of the dot product

$$\bar{A} = \bar{V}_{S\ell} \bullet \left[\nabla\bar{u}_\ell + (\nabla\bar{u}_\ell)^T - \frac{2\Delta}{3}\bar{\bar{I}}\right] = \bar{V}_{S\ell} \bullet 2\bar{\bar{S}}$$

$$= \Sigma_i\left\{\Sigma_j\left[\left(u_{gj} - u_{\ell j}\right)\left(\frac{\partial u_i}{\partial x_j} + \frac{\partial u_j}{\partial x_i}\right)\right] - \left(u_{gi} - u_{\ell i}\right)\frac{2\Delta}{3}\right\}\bar{\delta}_i, \tag{4.1.9}$$

(where $\bar{\delta}_i$ is the unit vector) are

$$A_x = \left(u_g - u_\ell\right)\left(2\frac{\partial u_\ell}{\partial x} - \frac{2}{3}\Delta\right) + \left(v_g - v_\ell\right)\left(\frac{\partial u_\ell}{\partial y} + \frac{\partial v_\ell}{\partial x}\right) + \left(w_g - w_\ell\right)\left(\frac{\partial u_\ell}{\partial z} + \frac{\partial w_\ell}{\partial x}\right), \tag{4.1.10a}$$

$$A_y = \left(u_g - u_\ell\right)\left(\frac{\partial u_\ell}{\partial y} + \frac{\partial v_\ell}{\partial x}\right) + \left(v_g - v_\ell\right)\left(\frac{2\partial v_\ell}{\partial y} - \frac{2}{3}\Delta\right) + \left(w_g - w_\ell\right)\left(\frac{\partial w_\ell}{\partial y} + \frac{\partial v_\ell}{\partial z}\right), \tag{4.1.10b}$$

and

$$A_z = (u_g - u_\ell)\left(\frac{\partial u_\ell}{\partial z} + \frac{\partial w_\ell}{\partial x}\right) + (v_g - v_\ell)\left(\frac{\partial v_\ell}{\partial z} + \frac{\partial w_\ell}{\partial y}\right) + (w_g - w_\ell)\left(2\frac{\partial w_\ell}{\partial z} - \frac{2}{3}\Delta\right). \quad (4.1.10c)$$

In addition, one has, for the denominator of the second term of Eq. 4.1.8,

$$S_{\ell m}S_{m\ell} = S_{11}^2 + S_{22}^2 + S_{33}^2 + 2S_{12}^2 + 2S_{13}^2 + 2S_{23}^2. \quad (4.1.11)$$

Equation 4.1.10 gives the components of the force acting on a single sphere (bubble or particle). Let N be the number of gas bubbles or particles in a cell of volume V_f. The gas volume in the cell is

$$V_g = \alpha_g V_f = N\frac{4}{3}\pi r_b^3 = N\frac{m_b}{\rho_b}, \quad (4.1.12)$$

where m_b and ρ_b are the average mass and density of a bubble. The force per unit volume acting on the bubbles is

$$F_{Li} = \frac{N L_i}{V_f} = \frac{N L_i \alpha_g}{V_g} = \frac{N L_i \alpha_g}{N\frac{4}{3}\pi r_b^3}$$

$$= \frac{6.46 \times 3}{4\pi}\frac{\alpha_g \rho_\ell \nu_\ell^{1/2}}{r_b} V_{S\ell j}\frac{2S_{ij}}{(2S_{\ell m}S_{m\ell})^{1/4}} \qquad (i, j = 1, 2, 3 = x, y, z)$$

$$= 6.17\frac{\alpha_g \rho_\ell \nu_\ell^{1/2}}{2r_b}\left\{\Sigma_j\left[(u_{gj} - u_{\ell j})\left(\frac{\partial u_i}{\partial x_j} + \frac{\partial u_j}{\partial x_i}\right)\right] - (u_{gi} - u_{\ell i})\frac{\Delta}{3}\right\}(2S_{\ell m}S_{m\ell})^{-1/4}. \quad (4.1.13)$$

The lift force acts in opposite directions upon the phases.

For cylindrical (r, θ, z) geometry, the components of the strain rate tensor $\overline{\overline{S}}$ are

$$S_{rr} = \frac{\partial u}{\partial r} - \frac{\Delta}{3}, \quad (4.1.14a)$$

$$S_{r\theta} = \frac{1}{2}\left[r\frac{\partial (v/r)}{\partial r} + \frac{1}{r}\frac{\partial u}{\partial \theta}\right], \quad (4.1.14b)$$

$$S_{rz} = \frac{1}{2}\left(\frac{\partial u}{\partial z} + \frac{\partial w}{\partial r}\right), \quad (4.1.14c)$$

$$S_{\theta\theta} = \frac{u}{r} + \frac{1}{r}\frac{\partial v}{\partial \theta} - \frac{\Delta}{3}, \quad (4.1.14d)$$

$$S_{\theta z} = \frac{1}{2}\left(\frac{1}{r}\frac{\partial w}{\partial \theta} + \frac{\partial v}{\partial z}\right), \quad (4.1.14e)$$

and

$$S_{zz} = \frac{\partial w}{\partial z} - \frac{\Delta}{3}. \tag{4.1.14f}$$

Hence, the components of the force per unit volume acting on the bubbles are

$$F_{Lr} = C\left\{\left(u_g - u_\ell\right)\left(2\frac{\partial u_\ell}{\partial r} - \frac{2\Delta}{3}\right) + \left(v_g - v_\ell\right)\left[r\,\frac{\partial(v_\ell/r)}{\partial r} + \frac{1}{r}\,\frac{\partial u_\ell}{\partial \theta}\right]\right.$$

$$\left. + \left(w_g - w_\ell\right)\left(\frac{\partial u_\ell}{\partial z} + \frac{\partial w_\ell}{\partial r}\right)\right\}, \tag{4.1.15a}$$

$$F_{L\theta} = C\left\{\left(u_g - u_\ell\right)\left[r\,\frac{\partial(v_\ell/r)}{\partial r} + \frac{1}{r}\,\frac{\partial u_\ell}{\partial r}\right] + \left(v_g - v_\ell\right)\left[2\left(\frac{u_\ell}{r} + \frac{1}{r}\,\frac{\partial v_\ell}{\partial \theta}\right) - \frac{2}{3}\,\Delta\right]\right.$$

$$\left. + \left(w_g - w_\ell\right)\left(\frac{1}{r}\,\frac{\partial w_\ell}{\partial \theta} + \frac{\partial v_\ell}{\partial z}\right)\right\}, \tag{4.1.15b}$$

$$F_{Lz} = C\left\{\left(u_g - u_\ell\right)\left(\frac{\partial u_\ell}{\partial z} + \frac{\partial w_\ell}{\partial r}\right) + \left(v_g - v_\ell\right)\left(\frac{1}{r}\,\frac{\partial w_\ell}{\partial \theta} + \frac{\partial v_\ell}{\partial z}\right)\right.$$

$$\left. + \left(w_g - w_\ell\right)\left(2\frac{\partial w_\ell}{\partial z} - \frac{2}{3}\,\Delta\right)\right\}, \tag{4.1.15c}$$

with

$$C = \frac{6.17\ \alpha_g \rho_\ell v_\ell^{1/2}/(2r_b)}{(2S_{\ell m}S_{m\ell})^{-1/4}}. \tag{4.1.16}$$

4.2 Drag Force

4.2.1 Bubbly Flow

The momentum exchange function K^M appearing on the right-hand side of momentum equation Eq. 3.1.2 is computed for bubbly flow as

$$K^M = \frac{3}{8}\,C_D\,\alpha_g \rho_\ell \frac{\left|\vec{V}_{S\ell}\right|}{r_b}, \tag{4.2.1.1}$$

with

$$C_D = \begin{cases} \dfrac{24}{Re_b}, & \text{if } Re_b < 1 \text{ (Stokes regime)} \\ \dfrac{24}{Re_b}\left(1 + 0.1\ Re_b^{0.75}\right), & \text{if } 1 < Re_b \le 5000 \text{ (viscous regime).} \\ 8/3. & \text{if } 5000 < Re_b \text{ (turbulent regime)} \end{cases} \quad (4.2.1.2)$$

The bubble Reynolds number Re_b has been defined by Eq. 3.2.3.1. The average radius of the bubbles is estimated assuming a Weber number

$$We = \frac{2r_b\rho_\ell|\vec{V}_{S\ell}|^2}{\sigma_{\ell g}} = 10, \quad (4.2.1.3)$$

where σ_{lg} (N/m) is the gas/water surface tension. The interfacial area, important because it can be evaluated experimentally and compared with calculations, is given (in bubbly flow) by

$$A_i = \frac{3\alpha_g}{r_b} \cdot \left(m^2/m^3\right). \quad (4.2.1.4)$$

4.2.2 Suspension Flow

The momentum exchange function is computed by[12]

$$K = \begin{cases} \dfrac{150}{\alpha_\ell}\dfrac{\alpha_g^2}{4}\dfrac{\mu_\ell}{r_b^2} + 1.75\dfrac{\rho_\ell\alpha_g|\vec{V}_{S\ell}|}{2r_b} & \text{if } \alpha_\ell \le 0.8 \\ \dfrac{3}{4}C_D\dfrac{\alpha_g\rho_\ell|\vec{V}_{S\ell}|}{2r_b}\alpha_\ell^{-2.7} & \text{if } \alpha_\ell > 0.8, \end{cases} \quad (4.2.2.1)$$

with

$$C_D = \begin{cases} \dfrac{24}{Re_p}\left(1 + 0.15Re_p^{0.687}\right) & \text{if } Re_p \le 1{,}000 \\ 0.44 & \text{if } Re_p > 1{,}000. \end{cases} \quad (4.2.2.2)$$

The particle Reynolds number is defined by

$$Re_p = \frac{2r_b\rho_\ell\alpha_\ell|\vec{V}_{S\ell}|}{\mu_\ell}. \quad (4.2.2.3)$$

The fluid viscosity μ_ℓ is taken to be a constant for isothermal flow. The solids viscosity μ_g is obtained from Krieger's[13] empirical expression for reduced viscosity η_r, given by

$$\eta_r = \frac{\alpha_g\mu_g + \alpha_\ell\mu_\ell}{\mu_\ell} = \left(1 - \frac{\alpha_g}{0.68}\right)^{-1.82}. \quad (4.2.2.4)$$

4.3 Virtual Mass Force

Let F_{vm} (N/m^3) be the virtual mass force for a unit volume of the carrying fluid, and f_{vm} (N) the virtual mass force acting on one particle. One has

$$\vec{f}_{vm} = \rho_f V_b C_{vm}\left(\frac{D\vec{u}_\ell}{Dt} - \frac{D\vec{u}_g}{Dt}\right) = \rho_f \frac{m_b}{\rho_b} C_{vm}\left(\frac{D\vec{u}_\ell}{Dt} - \frac{D\vec{u}_g}{Dt}\right)$$

$$= \frac{\rho_f}{\rho_b} m_b C_{vm}\left[\frac{\partial \vec{u}_\ell}{\partial t} + \vec{u}_\ell \bullet \nabla\vec{u}_\ell - \left(\frac{\partial \vec{u}_g}{\partial t} + \vec{u}_g \bullet \nabla\vec{u}_g\right)\right] \qquad (4.3.1)$$

and

$$\vec{F}_{vm} = \frac{N\vec{f}_{vm}}{V} = n\vec{f}_{vm} = n m_b \frac{\rho_f}{\rho_b} C_{vm}\vec{a}_{vm} = \alpha_b \rho_f C_{vm}\vec{a}_{vm}, \qquad (4.3.2)$$

having used $nm_b = \alpha_b \rho_b$ and the definition of virtual mass acceleration

$$\vec{a}_{vm} = \frac{D\vec{u}_\ell}{Dt} - \frac{D\vec{u}_g}{Dt}. \qquad (4.3.3)$$

Hence, for every coordinate direction i (= x, y, z), the component of the virtual mass force is

$$F_{vm,i} = \alpha_b \rho_f C_{vm}\left[\frac{\partial u_{\ell i}}{\partial t} + u_{\ell j}\frac{\partial u_{\ell i}}{\partial x_j} - \left(\frac{\partial u_{gi}}{\partial t} + u_{gj}\frac{\partial u_{gi}}{\partial x_j}\right)\right]. \qquad (4.3.4)$$

For spherical particles or nondeformable bubbles, the theoretically derived value for C_{vm} is 0.5. Experiments performed by Odar[14] suggest that C_{vm} can be a function of the acceleration modulus

$$C_{vm} = 1.05 - \frac{0.66}{A_c^2 + 0.012}, \qquad (4.3.5)$$

with A_c, the acceleration modulus, given by

$$A_c = \frac{\left|\vec{u}_\ell - \vec{u}_g\right|^2}{|\vec{a}_{vm}| d_b}. \qquad (4.3.6)$$

So far, $C_{vm} = 0.5$ has been used in the code for liquid–solids flow and bubbly flow.

5 First Assessment of Computations for Turbulent Bubbly Flow

5.1 Comparison of COMMIX-M-Calculated Results with Experimental Results of Simonin and Viollet

Results of numerical computations of turbulent bubbly flow in a vertical axisymmetric pipe, reported in Ref. 15, have been chosen for comparison with results obtained with the COMMIX–M code. The simulated test section consists of a pipe of 50 mm internal diameter and 4 m length. Two runs of upward flow, with the characteristics given in Table 1, have been computed. The injection of air bubbles, 2 mm in diameter, is assumed to be uniformly distributed at the inlet. Calculations with COMMIX–M have been made with 20 radial and 25 axial uniform meshes. The results reported in Ref. 15 and those obtained with COMMIX–M are presented in Figs. 3-10. Figures 3–6 refer to Run No. 1, and Figs. 7–10 to Run No. 2. All figures present distributions at the same axial level.

Figure 3 indicates that the COMMIX–M calculation fails, so far, to reproduce the sink of the air volume fraction at the wall, whereas Figs. 4 and 5 show that COMMIX-M results for radial distributions of water velocity and air velocity agree reasonably well with the results of Simonin and Viollet.[15]

Radial distributions of turbulence kinetic energy in the water phase (Fig. 6) underestimate the production of turbulence kinetic energy near the wall. The results obtained from Run No. 2 (Figs. 7-10) are similar to those obtained from Run No. 1. Further comments and conclusions will be drawn when models are improved and more computations are available.

5.2 Comparison of COMMIX-M-Calculated Results with Experimental Results of NOVA Test Series

Preliminary results of the computation of the NOVA test series performed at the Kernforschungszentrum Karlsruhe (KfK)[16] were obtained for the test runs shown in Table 2. The experiments were run in a vertical pipe of 70 mm inner diameter and 5 m length. The geometry was simulated with 20 uniform meshes of 1.75 mm in the radial direction and 25 uniform meshes 0.16 m in length (for a total length of 4 m) in the axial direction.

Experimental data for the two runs are available only for the void fraction. Some preliminary results of the computations are shown in Figs. 11 and 12 for Run No. 1 and in Figs. 13 and 14 for Run No. 3.

Experimental evaluations of water and air velocities are not available at this time. A comparison of experimental and computed results is possible now only for the void distributions shown in Figs. 11 and 13 for Runs 1 and 3, respectively. Both figures show that the maxima of air volume fraction compare well in experiments and calculation, but that the distributions near the wall are very different. The experimental results show a peak close to the wall, whereas the computed results predict a sink of the void profile before the maximum value. This maximum value is also closer to the wall than in the experimental data. The reason for this discrepancy is likely to depend on the computed pressure radial profiles and on the resulting lift forces. The problem is under investigation.

Table 1. Characteristics at inlet for computed turbulent bubbly flow experiments reported by Simonin and Viollet[15]

Characteristics		Run No. 1	Run No. 2
Volumetric flux (m/s):	Water j_l	0.87	0.87
	Air j_g	0.005	0.10
Velocity (m/s):	Water w_l	0.92	0.97
	Air w_g	0.92	0.97
Density (kg/m^3):	Water ρ_l	997	997
	Air ρ_g	1.18	1.18
Mass flow (kg/s):	Water G_l	1.703	1.703
	Air G_g	1.158×10^{-4}	2.317×10^{-4}
Volumetric flow rate (m^3/s):	Water Q_l	1.708×10^{-3}	1.708×10^{-3}
	Air Q_g	9.817×10^{-5}	1.963×10^{-4}
Flowing quality:	Water x_l	0.999932	0.999864
	Air x_g	0.000068	0.000136
Volume fractions:	Water α_l	0.9456	0.8969
	Air α_g	0.0544	0.1031

Table 2. Characteristics at inlet of two simulated test runs of NOVA series

Characteristics		Run No. 1[a]	Run No. 3[a]
Velocity (m/s):	Water w_l	1.86	2.04
	Air w_g	2.28	2.50
Mass flow (kg/s):	Water G_l	6.944	6.944
	Air G_g	7.2×10^{-4}	2.41×10^{-3}
Flow quality:	Water x_l	0.999948	0.999827
	Air x_g	0.000052	0.000173
Volume fraction:	Water α_l	0.959	0.874
	Air α_g	0.041	0.126

[a]Volumetric flow rate $Q_l = 25$ m^3/h.

6 First Assessment of Computations of Turbulent Particulate Flow

6.1 Numerical Computation of Attenuation of Turbulent Kinetic Energy for Small Particles

The attenuation of turbulent kinetic energy due to small particles has been investigated numerically using the modeling approach explained in Section 3.2.3. For this purpose, an independent computer program called PARTVI has been used. The list of the program is given for reference in the Appendix. Assuming that particles of density $\rho_b = 1000\ kg/m^3$ are transported by air flow ($\rho_\ell = 1{\cdot}2\ kg/m^3$, $\nu_\ell = 1.57 \times 10^{-5}\ m^2/s$), we have computed three cases with particle volume fractions $\alpha_b = 0.01/0.005/0.001$, respectively. The corresponding mean concentrations of the particles are $W = \alpha_b\rho_b/(\alpha_b\rho_b + \alpha_\ell\rho_\ell) = 0.894/0.807/0.455$. Particle diameter ranged from 0.1 to 3 mm in steps of 0.1 mm. The integral attenuations, defined by Eq. 3.2.3.32, are shown versus the particle diameter in Fig. 15. For particles with large diameters, the attenuation factor approaches the limit value of 1. Similarly, for very small particles ($\alpha_b < 10^{-6}$) there is practically no attenuation. Between these limit values, the plots show very strong attenuation in the range between $\alpha_b = 0.1$ and $\approx$1.5 mm.

A subroutine based on the approach used in the PARTVI program has been linked to the COMMIX-M code and has been used for the case of particle Reynolds number smaller than 110. This is the case for the numerical computation of one of the test cases discussed in the next section.

6.2 Comparison of COMMIX-M-Calculated Results with Experimental Results of Tsuji, Morikawa, and Shiomi

Measurements of air and solid particle velocities in a vertical pipe of 30.5 mm inner diameter have been reported in Ref. 17 for spherical particles with diameters ranging from 0.2 to 3 mm. Particle density ranged from 970 to 1030 kg/m^3. The value $\rho_b = 1000\ kg/m^3$ has been used in the calculations. It was confirmed experimentally that the presence of large particles enhances the turbulent kinetic energy of the carrying flow, while small particles damp the turbulence. From the several runs of the experimental series, four test cases have been selected for the numerical calculations. The main characteristics of these test cases are summarized in Table 3, where A denotes the cross-flow area of the pipe. Test case 1 is a reference case without particles and gives information about the intensity of the turbulent kinetic energy of the undisturbed main air flow. In test cases 2 and 3, with large transported particles of 3 mm diameter, the intensity of turbulent kinetic energy is expected to increase with respect to the reference case because of the presence of the particles. Conversely, in test case 4, with small particles of 0.2 mm diameter, the intensity of turbulent kinetic energy is expected to be damped by the particles.

A comparison between experimental and computed results is shown in the reference test case 1 without particles (m = 0) in Fig. 16. The intensity of turbulence associated with the oscillations of the velocity component in the axial direction w' is normalized to the axial air velocity W_c. The results of two calculations are shown: the first calculation was performed with the COMMIX-1C code by using the K-ε model. Thus w' is replaced by $(2K/3)^{1/2}$, assuming isotropic turbulence. The computed results are in good agreement with the experimental values at the pipe axis, but show a deviation of $\approx$20% at the wall; the

Table 3. Characteristics of computed experiments from Tsuji, Morikawa, and Shiomi series

	Test Case			
Characteristic	1	2	3	4
Particle diameter d_b (mm)	-	3	3	0.2
Particle volume fraction α_b	0	0.00072	0.004	0.0016
Loading ratio $m = \alpha_b\rho_b/\alpha_\ell\rho_\ell$	0	0.6	3.4	1.3
Inlet axial mean velocity $\overline{W}$ (m/s)	11.1	12.1	11.8	10.7
Particle volumetric flow $Q_b = \overline{W}\alpha_b A(m^3/s)$	0	5.95×10^{-6}	3.41×10^{-5}	1.20×10^{-5}
Air volumetric flow $Q_\ell = \overline{W}\alpha_\ell A(m^3/s)$	7.84×10^{-3}	8.26×10^{-3}	8.30×10^{-3}	7.49×10^{-3}
Particle mass flow $G_b = \rho_b Q_b$ (kg/s)	0	5.95×10^{-3}	3.41×10^{-2}	1.20×10^{-2}
Air mass flow $G_\ell = \rho_\ell Q_\ell$ (kg/s)	9.41×10^{-3}	9.91×10^{-3}	9.96×10^{-3}	8.99×10^{-3}
Particle mass fraction $x_b = G_b/(G_b + G_\ell)$	0	0.375	0.774	0.571
Air mass fraction $x_\ell = G_\ell/(G_b + G_\ell)$	1	0.625	0.226	0.429
Maximum computed slip velocity $\lvert Vs_\ell \rvert$ (m/s)	-	2.98	3.48	0.6
Maximum particle Reynolds number $Re_b = \frac{d_b\rho_\ell\lvert V_{s\ell}\rvert}{\mu_\ell}$	-	569	665	8

second calculation was performed with the COMMIX-M code by using the Reynolds Stress Model (RSM). The RSM shows better agreement close to the wall but a deviation of ≈30% at the pipe center.

A comparison between experimental and computed normalized turbulence intensity of air is shown in Fig. 17 for test case 2 with loading ratio m = 0.6. Compared with the case with m = 0, we see that the turbulence intensity is increased by almost 50% at the pipe center and by ≈10% at the wall. In this case, agreement between experimental and

computed results is very good at the pipe center, while at the wall the computed intensity of the turbulence is underpredicted by 10-15%.

A further increase of turbulence intensity with respect to the reference case is observed in test case 3, as shown in Fig. 18. The turbulence intensity at the pipe center is more than doubled, while at the wall the increase is smaller (≈15%). As in the previous case, agreement between experiment and calculation is good at the pipe center while the computed values are underpredicted as we proceed toward the pipe wall.

The normalized axial velocities of air and particles for test case 3 are shown in Fig. 19. While there is no comparison with experimental data, the information is given for future reference. It is also relevant to estimate the particles Reynolds number, which is based on the slip velocity.

Figure 20 shows a comparison of experimental and computed intensity of turbulence for test case 4 with the small particles of 0.2 mm diameter. The plot labeled m = 0 refers to air flow without particles, but with the same mass velocity $\overline{W}$ = 10.7 (which is less than in the reference test case 1). Presence of the small particles damps the turbulence intensity at the pipe center by ≈30%, while at the wall there is no or negligible damping. The computed results agree with the experimental ones at the pipe center and at the wall, but the distribution between shows considerable deviations.

Normalized velocity distributions for the test case 4 are shown in Fig. 21. Computed and experimental values for the air flow compare very well from the pipe axis to r/R = 0.8, while some discrepancy remains at the wall.

7 Data Analysis

A program called PROCESS has been linked to COMMIX-M to compute the energy spectral distribution of the velocity fluctuations in three coordinate directions and to compute the crosscorrelations of any two signals.

In the course of a time-dependent calculation made with COMMIX-M, selected data, e.g., u_i (i = x, y, z), T, K_l, etc., were written into a DATABASE file, which consists typically of values taken at some thousands of time points. PROCESS reads the DATABASE file and processes the information in a sequence of blocks of given length L (i.e., blocks consisting of values referring to L time points). L, which must be a power of 2, is typically 256.

For every block of data of length L, velocity components are first processed to compute their energy spectra. The calculations proceed as described below.

Let $\tilde{u}(t)$, $\overline{u}$, and u(t) be the instantaneous value, mean value over a block of length L, and fluctuation from the mean value of a velocity component, respectively, therefore

$$\tilde{u}(t) = \overline{u} + u(t). \qquad (7.1)$$

First, the momenta of $\tilde{u}(t)$ are computed, namely,

$\overline{u}$ = Mean value

$\sigma^2 = \overline{u^2}$ = Variance

σ = Standard Deviation

$S = \dfrac{\overline{u^3}}{\sigma^3}$ = Skewness

$Ku = \dfrac{\overline{u^4}}{\sigma^4}$ = Kurtosis.

Hence, the velocity fluctuations u(t) are computed from Eq. 6.1.

Then, the autocorrelation of the signal u(t) is computed as

$$\rho(\tau) = \frac{1}{\overline{u^2}}\,\overline{u(t)u(t')}, \tag{7.2}$$

with $\tau = t' - t$. The Fourier transform of the autocorrelation then gives the power spectral density, or energy spectrum

$$S(\omega) = \frac{1}{2\pi}\int_{-\infty}^{+\infty} e^{-i\tau\omega}\rho(\tau)d\tau. \tag{7.3}$$

Its antitransform is

$$\rho(\tau) = \int_{-\infty}^{+\infty} e^{i\tau\omega}S(\omega)d\omega. \tag{7.4}$$

PROCESS also computes, if required, the crosscorrelations of different signals at the same location or of the same signal at different locations. The crosscorrelation of two signals $u_1(t)$, $u_2(t)$ is given by

$$\rho_{1-2}(\tau) = \frac{1}{\sigma_1\sigma_2}\,\overline{u_1(t)u_2(t')}. \tag{7.5}$$

A simplified flow chart of PROCESS is shown in Fig. 22.

Acknowledgments

This work has been sponsored by the U.S. Department of Energy, Pittsburgh Energy Technology Center. The authors express their gratitude to Ms. S. Moll and Ms. J. Fisher for their accurate work in typing the manuscript.

References

1. Y. A. Hassan, Implementation of a Mass–Flow–Weighted Skew–Upwind Differencing Scheme in COMMIX–1A, Electric Power Research Institute Report EPRI NP–3518 (1984).

2. S. C. Eisenstat, M. C. Gursky, M. H. Schultz, and A. H. Sherman, *Yale Sparse Matrix Package, II. The Nonsymmetric Codes*, Research Report #114, Dept. of Computer Science, Yale University (1977).

3. H. C. Elman, *Iterative Methods for Large, Sparse, Nonsymmetric Systems of Linear Equations*, Ph.D. Dissertation, Yale University (May 1982).

4. M. Bottoni et al., COMMIX–M manual, draft of internal report, unpublished (1993).

5. J. Ding et al., *Analysis of Liquid–Solids Suspension Velocities and Concentrations Obtained by NMR Imaging*, NSF–DOE Workshop on Flow of Particles and Fluids, Gaithersburg, MD (Sept. 17–18, 1992).

6. H. M. Domanus, et al., *COMMIX–1C: A Three–Dimensional Transient Single–Phase Computer Program for Thermal Hydraulic Analysis of Single and Multicomponent Systems, Vol. I, Equations and Numerics; Vol. II, User's Manual*, NUREG/CR–5649, Argonne National Laboratory Report ANL–90–33 (Nov. 1990).

7. M. Bottoni and F. C. Chang, *Implementation of an Anisotropic Turbulence Model in the COMMIX–1C/ATM Computer Code*, ASME Pressure Vessel and Piping (PVP) Division Conference, Denver, CO (July 25–29, 1993).

8. A. M. Al Taweel and J. Landau, *Turbulence Modulation in Two-Phase Jets*, Int. J. Multiphase Flow, Vol. 3, 341-351 (1977).

9. S. L. Lee and M. A. Wiesler, *Theory on Transverse Migration of Particles in a Turbulent Two-Phase Suspension Flow Due to Turbulent Diffusion - I*, Int. J. Multiphase Flow, Vol. 13. 99-111 (1987).

10. H. Tennekes and J. L. Lumley, *A First Course in Turbulence*, the MIT Press, Cambridge, MA (1972).

11. P. G. Saffman, *The Lift on a Small Sphere in a Slow Shear Flow*, J. Fluid Mech., 22, Part 2, 385–400 (1965).

12. R. B. Bird, W. E. Stewart, and E. N. Lightfoot, *Transport Phenomena*, John Wiley, New York (1960).

13. I. M. Krieger, Adv. Colloid Interface Sci., 3, 111 (1972).

14. F. Odar, *Verification of Proposed Equation for Calculation of Forces on a Sphere Accelerating in a Viscous Fluid*, J. Fluid Mech. 25, 591–592 (1966).

15. O. Simonin and P. L. Viollet, *Numerical Study on Phase Dispersion Mechanisms in Turbulent Bubbly Flows*, Int. Conf. on Mechanics of Two–Phase Flows, National Taiwan University, Taipei (June 12–15, 1989).

16. Private communication of preliminary data by Dr. W. Sengpiel, Kernforschungszentrum, Karlsruhe, Germany (1991).

17. Y. Tsuji, Y. Morikawa, and H. Shiomi, *LDV Measurements of an Air-Solid Two-Phase Flow in a Vertical Pipe*, J. Fluid Mech., 139, 417-434 (1984).

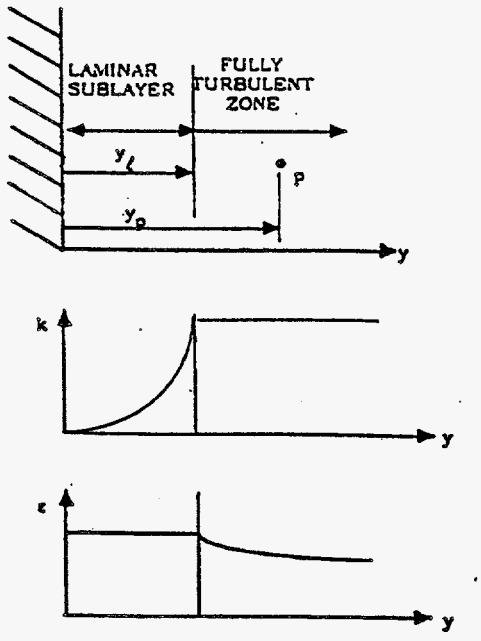

Fig. 1. Two-layer wall function model ($y_p > y_l$)

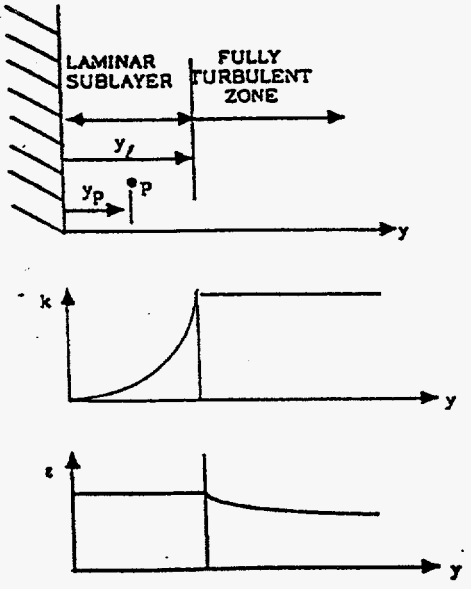

Fig. 2. Two-layer wall function model ($y_p \leq y_l$)

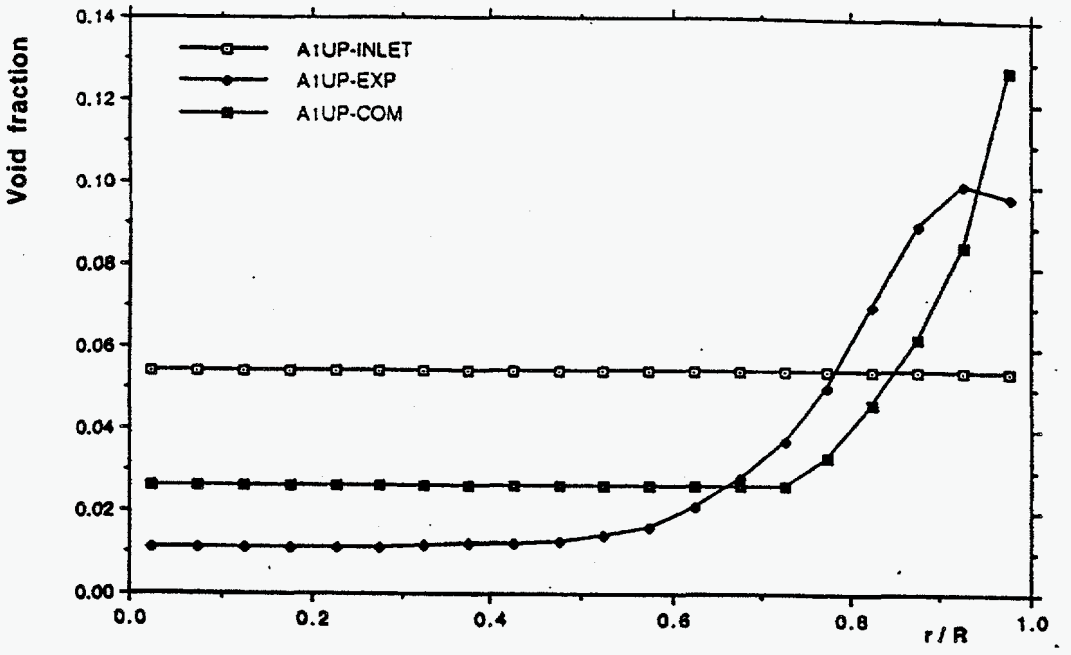

Fig. 3. *Run No. 1: radial distribution of air volume fraction at inlet, and comparison of Simonin–Viollet[15] data (EXP) with COMMIX–M computation (COM) at z = 3.12 m.*

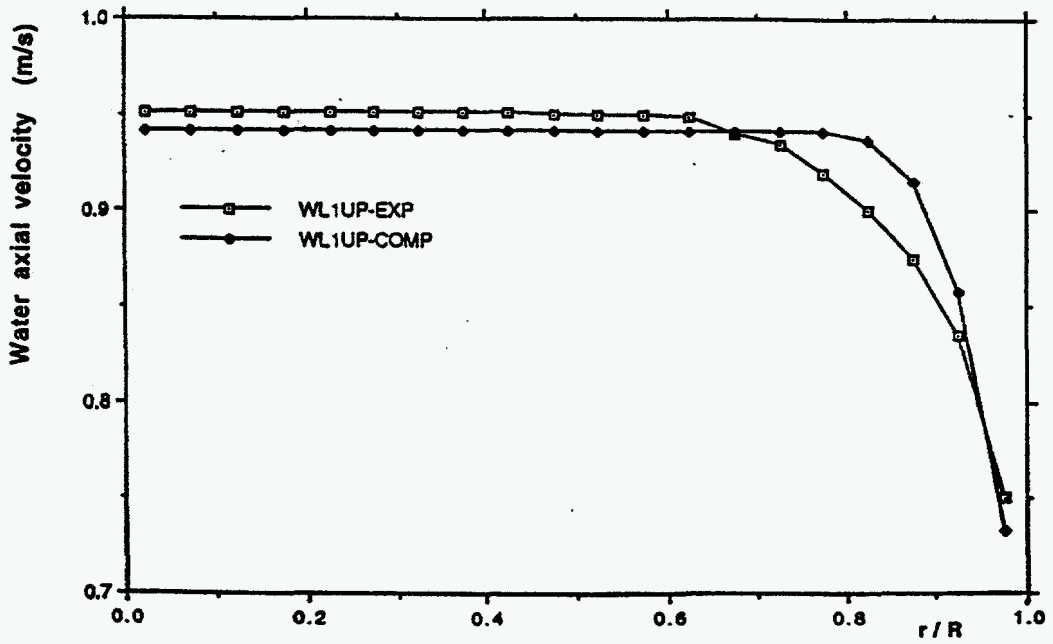

Fig. 4. *Run No. 1: radial distribution of water axial velocity at z = 3.12 m. Comparison of Simonin–Viollet[15] data (EXP) with COMMIX–M computation (COM).*

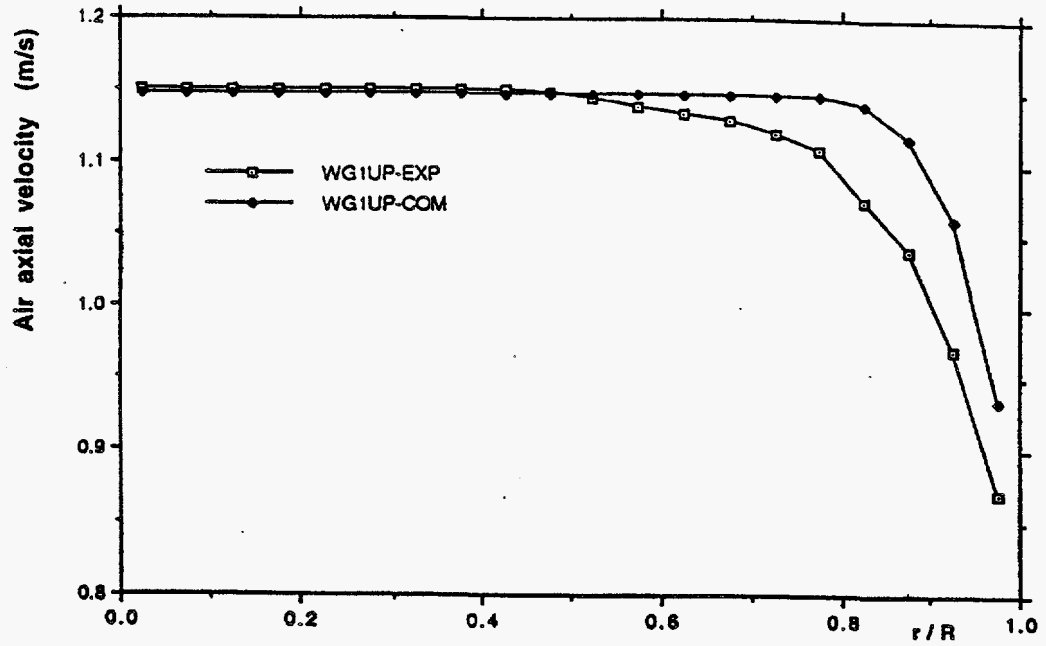

Fig. 5. Run No. 1: radial distribution of air axial velocity at z = 3.12 m. Comparison of Simonin–Viollet[15] data (EXP) with COMMIX–M computation (COM).

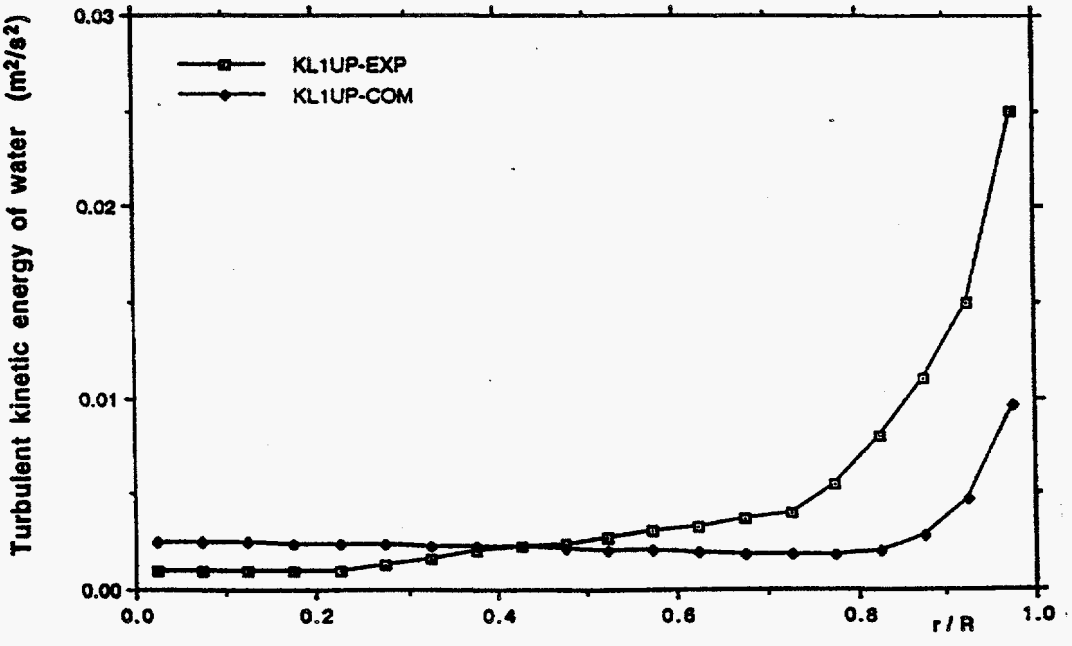

Fig. 6. Run No. 1: radial distribution of turbulence kinetic energy of water phase at z = 3.12 m. Comparison of Simonin–Viollet[15] data (EXP) with COMMIX–M computation (COM).

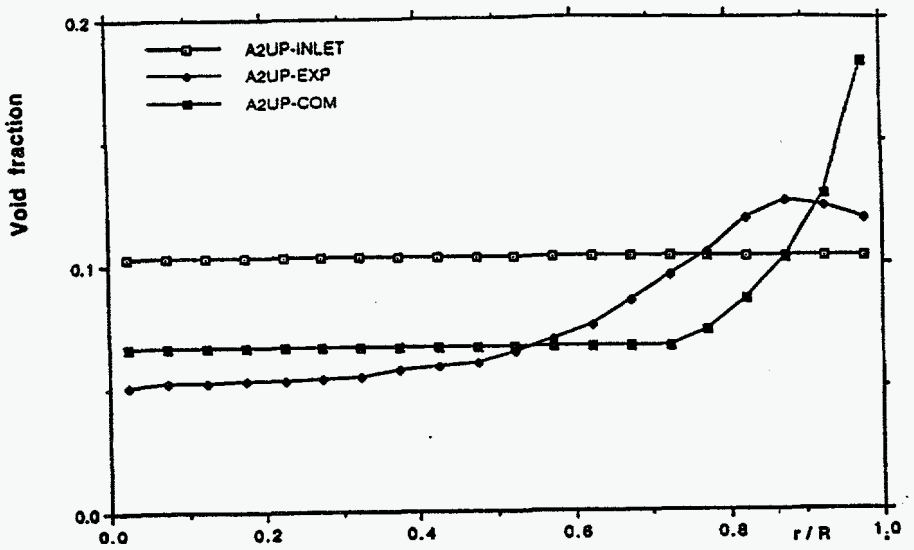

Fig. 7. Run No. 2 : radial distribution of void fraction at inlet, and comparison of Simonin–Viollet[15] data (EXP) with COMMIX–M computation (COM) at z = 3.12 m.

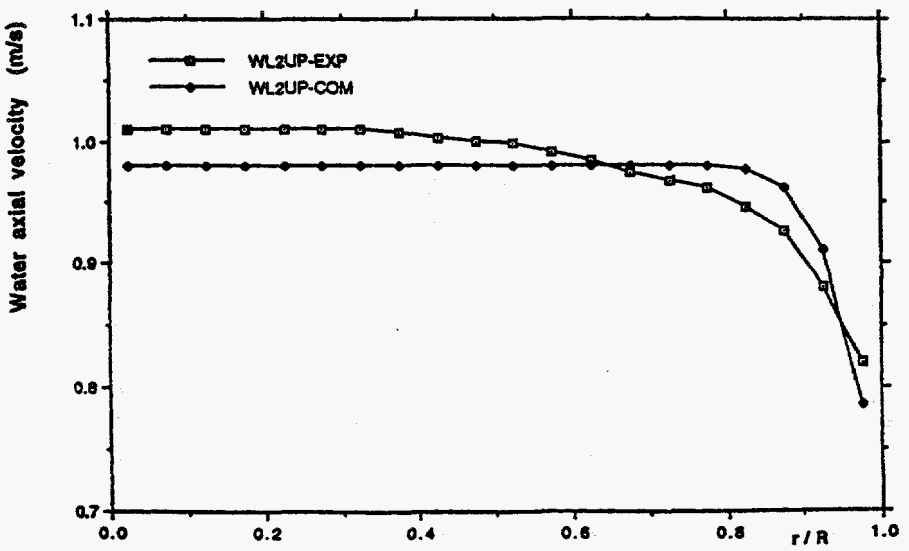

Fig. 8. Run No. 2: radial distribution of water axial velocity at z = 3.12 m. Comparison of Simonin–Viollet[15] data (EXP) with COMMIX–M computation (COM).

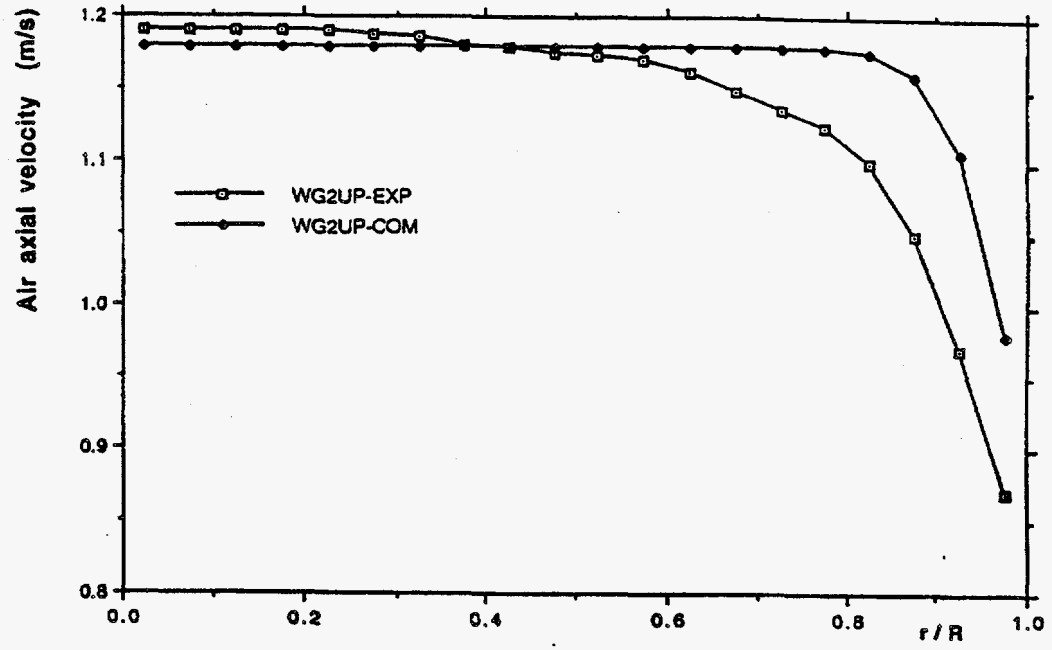

Fig. 9. Run No. 2: radial distribution of air axial velocity at z = 3.12 m. Comparison of Simonin–Viollet[15] data (EXP) with COMMIX–M computation (COM).

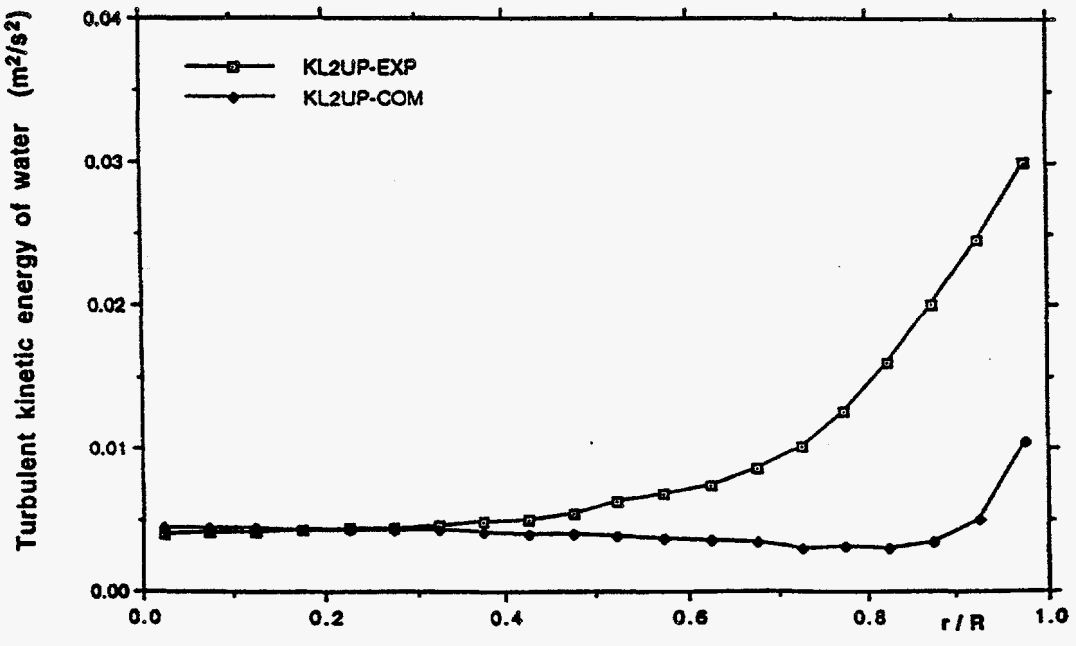

Fig. 10. Run No. 2: radial distribution of turbulence kinetic energy of water phase at z = 3.12 m. Comparison of Simonin–Viollet[15] data (EXP) with COMMIX–M computation (COM).

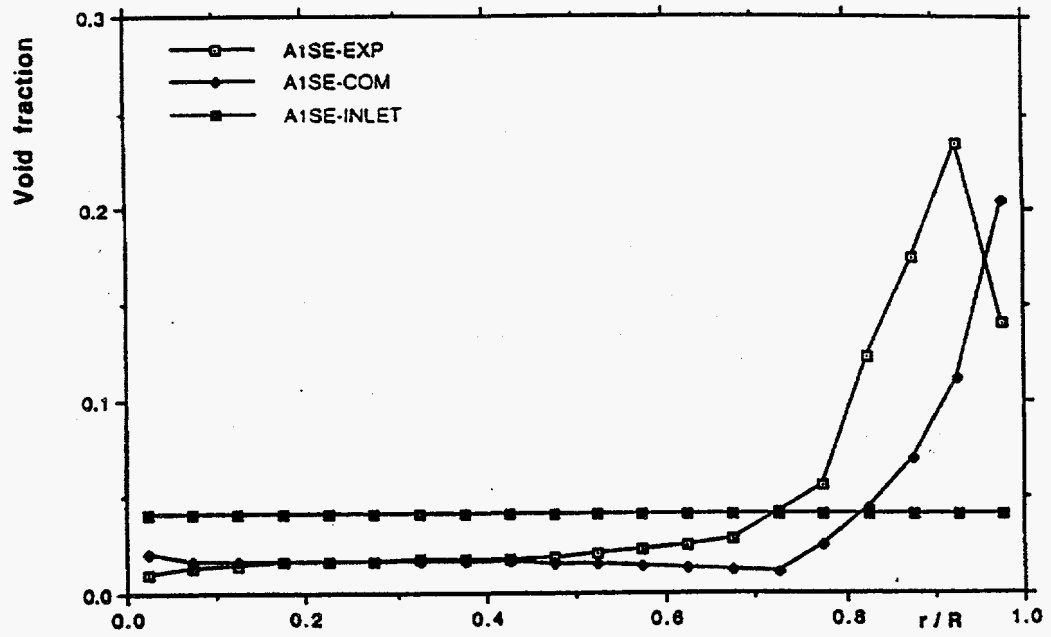

Fig. 11. NOVA test series, Run No. 1: radial distribution of void fraction at inlet, and comparison of experimental data from the NOVA test series[16] (EXP) with COMMIX-M computation (COM).

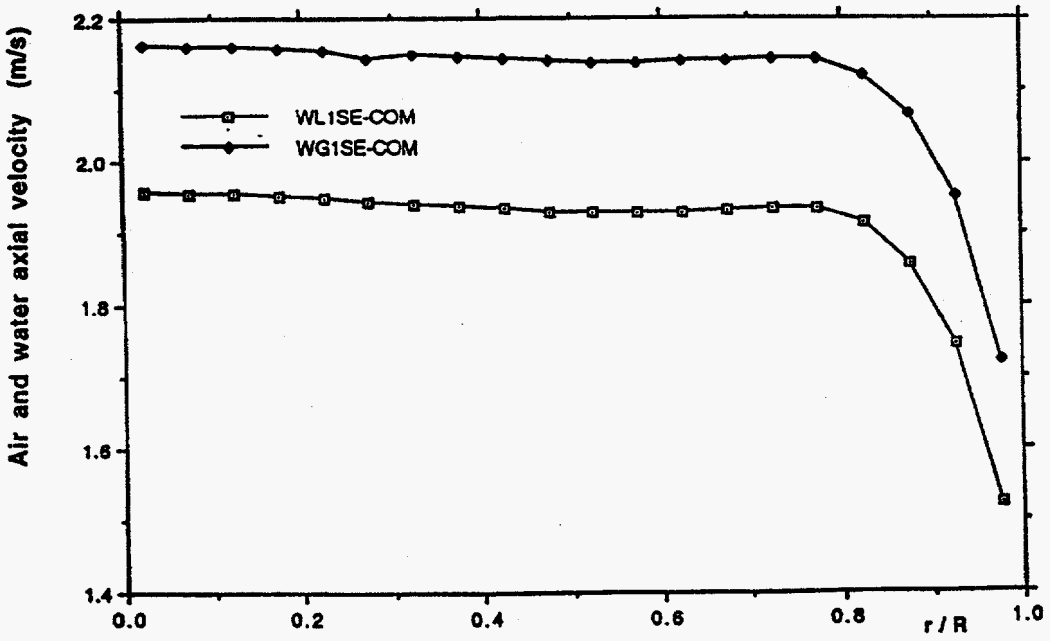

Fig. 12. NOVA test series, Run No. 1: computed radial distributions of air (WG) and water (WL) axial velocities.

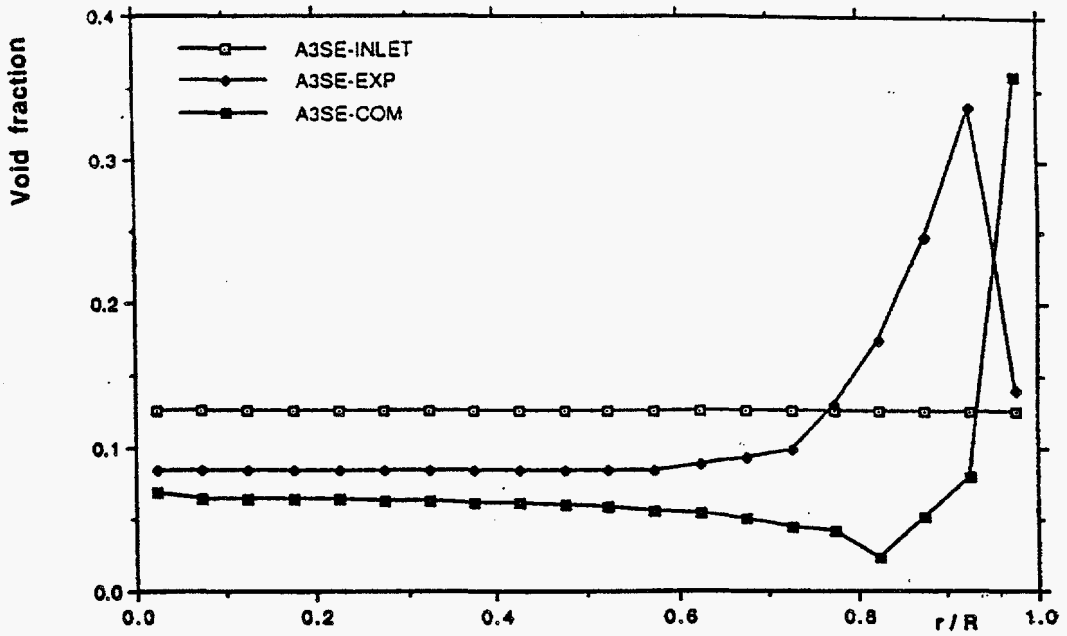

Fig. 13. NOVA test series, Run No. 3: radial distribution of void fraction at outlet, and comparison of experimental data from NOVA test series (EXP) with COMMIX–M computation (COM).

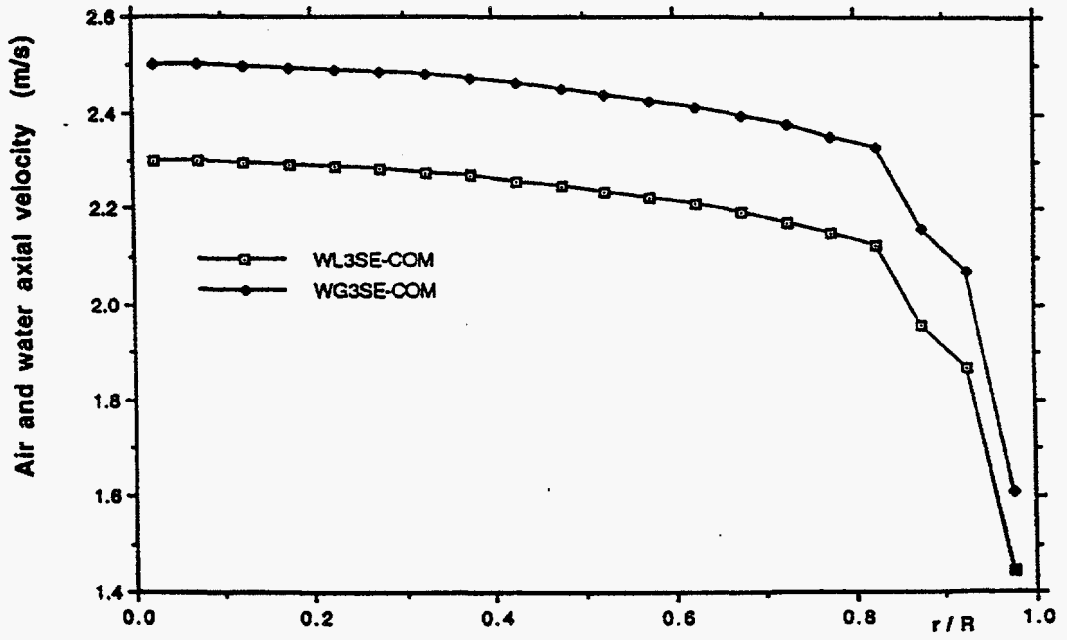

Fig. 14. NOVA test series, Run No. 3: computed radial distributions of air (WG) and water (WL) axial velocities.

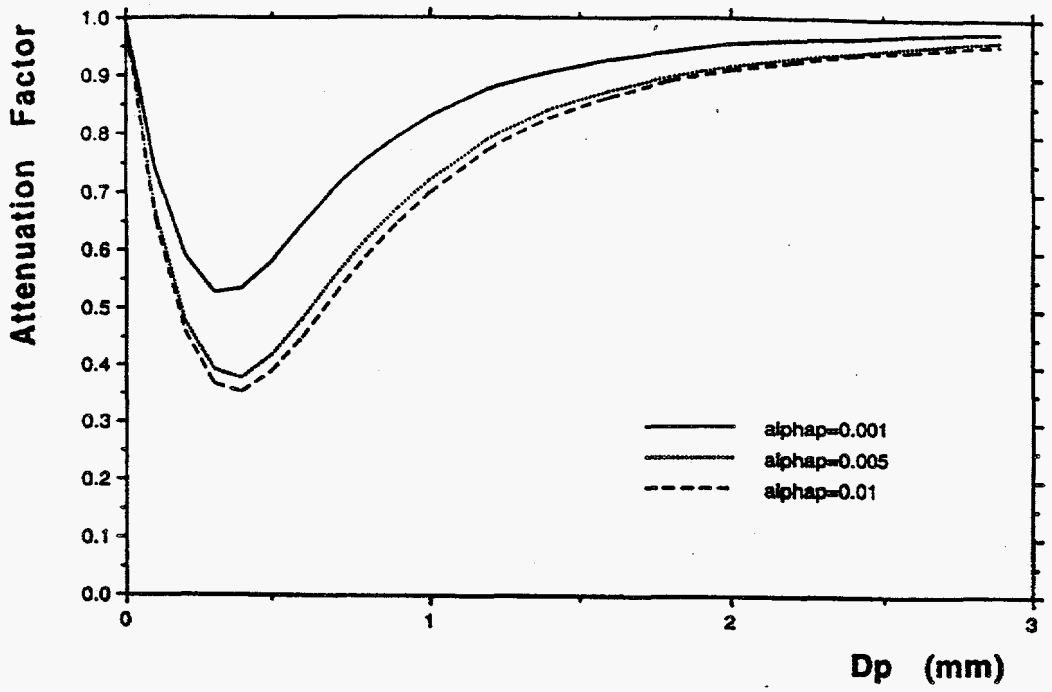

Fig. 15. Attenuation of turbulence intensity due to particles vs. particle diameter.

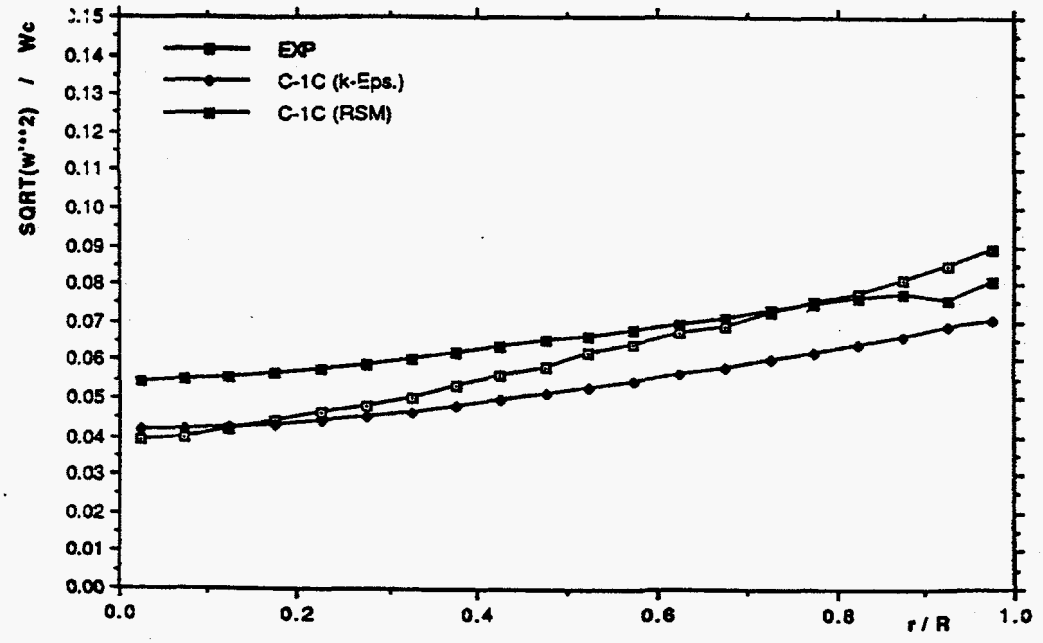

Fig. 16. Radial distribution of turbulence intensity for test case 1 of Tsuji-Morikawa-Shiomi experiments.

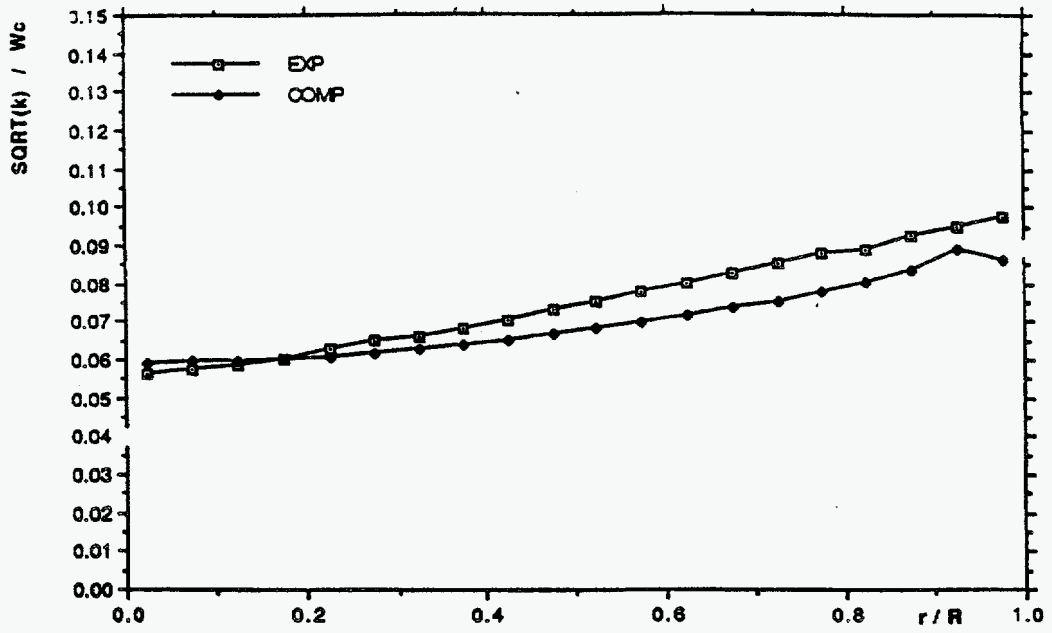

Fig. 17. Radial distribution of turbulence intensity for test case 2 of Tsuji-Morikawa-Shiomi experiments.

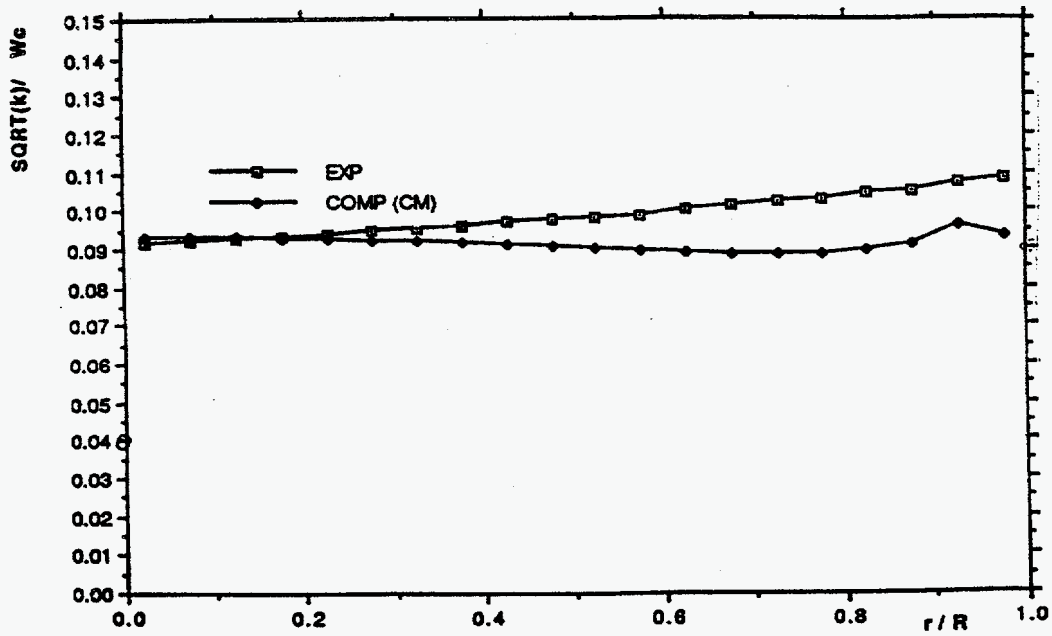

Fig. 18. Radial distribution of turbulence intensity for test case 3 of Tsuji-Morikawa-Shiomi experiments.

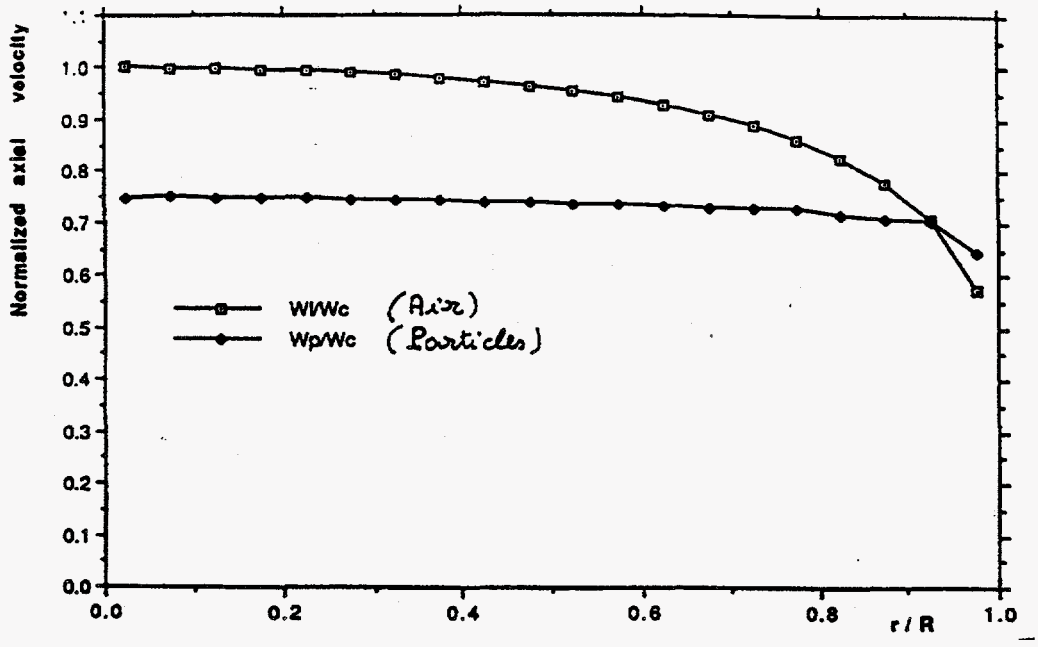

Fig. 19. Radial distribution of normalized axial velocity for test case 3 of Tsuji-Morikawa-Shiomi experiments.

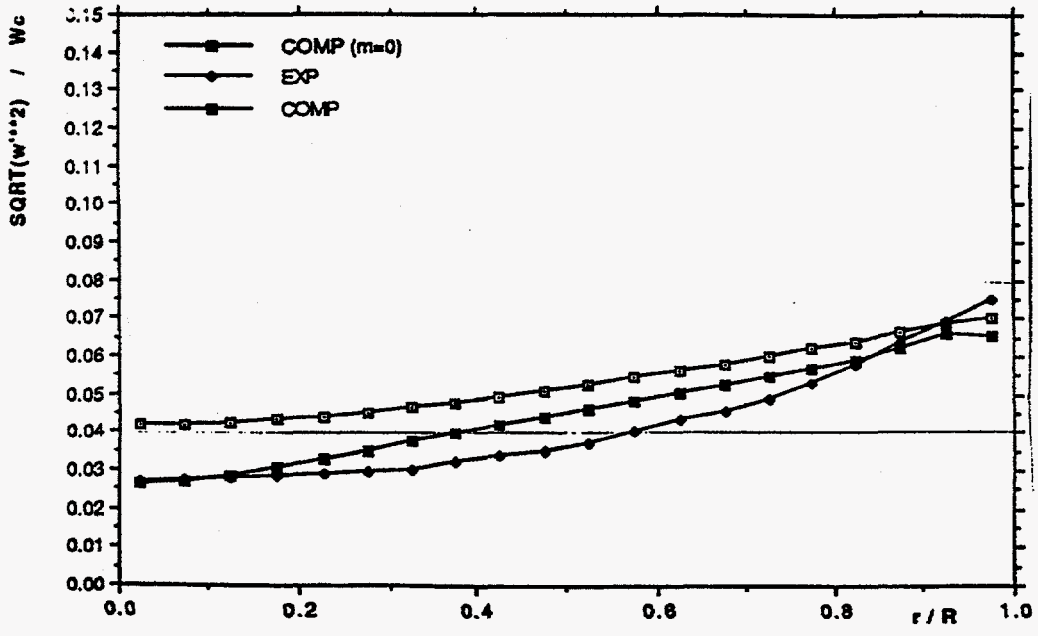

Fig. 20. Radial distribution of turbulence intensity for test case 4 of Tsuji-Morikawa-Shiomi experiments.

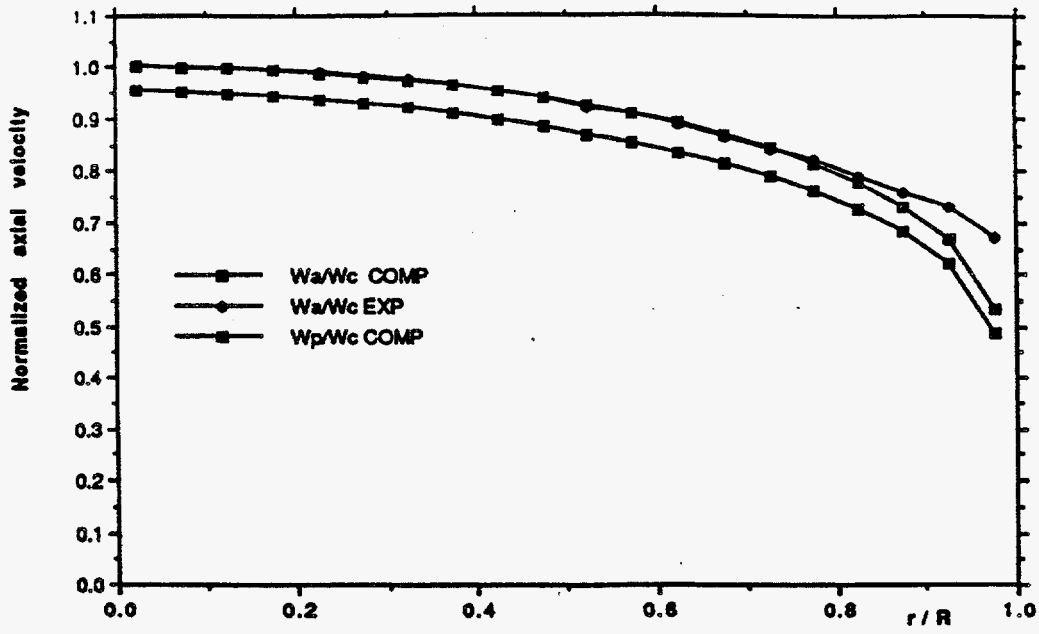

Fig. 21. Radial distribution of normalized axial velocity for test case 4 of Tsuji-Morikawa-Shiomi experiments.

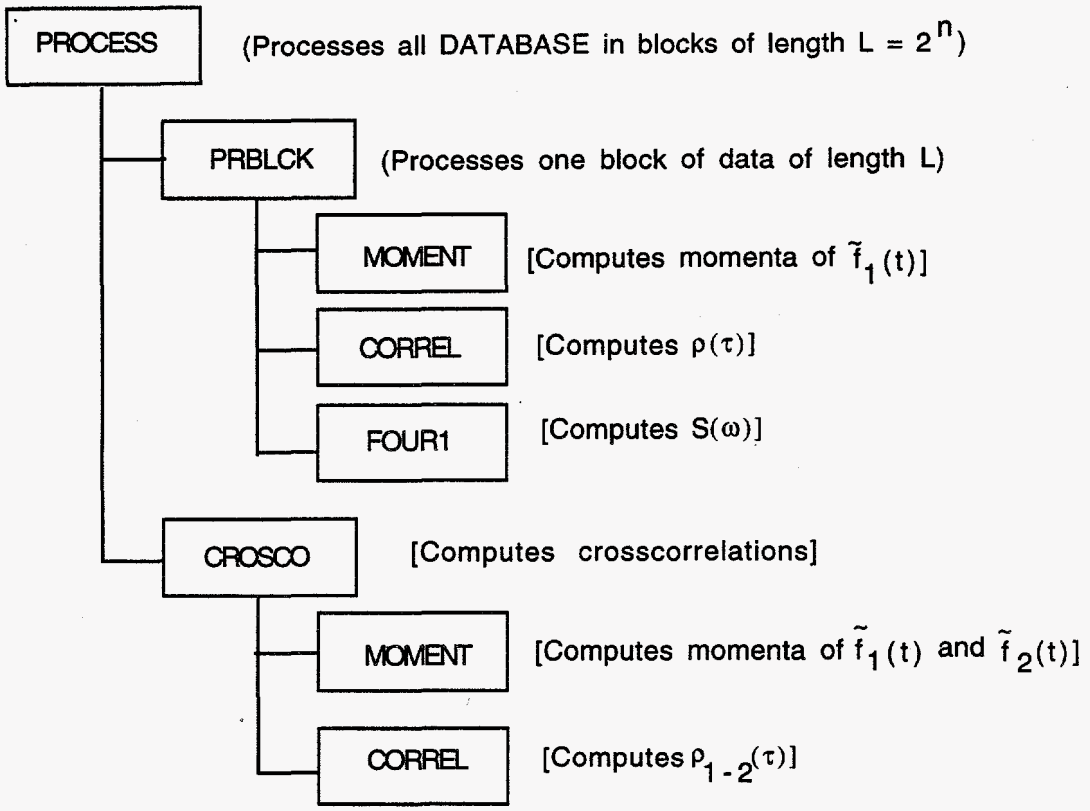

Fig. 22. Simplified flow chart of PROCESS program, used for data analysis

Appendix I: List of Program PARTVI

```
c     MAIN - PROGRAM PARTVI
c     Main program to compute the attenuation of turbulent kinetic
c     energy of a carrying fluid due to small particles.
c
c     ------------------------------------------------------------
c     Definition of variables
c
c     alphaf = volume fraction of carrying fluid;
c     alphap = volume fraction of particles;
c     anuf   = kinematic viscosity of carrying fluid (m**2/s);
c     diap   = particle diameter (m);
c     eta    = Kolmogorov microscale of length (m);
c     hkmean = mean value of the attenuation of the turbulent kinetic
c              energy;
c     rhof   = density of carrying fluid (kg/m**3);
c     rhop   = density of particles (kg/m**3);
c     tdcomp = dissipation of turbulent kinetic energy in the carrying
c              fluid (m**2/s**3);
c     tkcomp = turbulent kinetic energy of the carrying fluid in absence
c              of particles (m**2/s**2);
c     vel    = velocity of carrying fluid (m/s);
c     ------------------------------------------------------------
c
      implicit real*8 (a-h, o-z)
c
      open(6,file='OUTPUT',status='unknown')
c
c     ------------------------------------
c     In the application of the subroutines given below it is assumed
c     that the constants given here, as well as the particle diameter,
c     are transferred from a driver program.
      tkcomp=0.2d0
      tdcomp=10.d0
      rhop=1000.d0
      rhof=1.2d0
      anuf=1.57d-05
      alphap=0.0050d0
c     ------------------------------------
c
      do 800 iloop=1,30
      diap= float(iloop-1)*100.d-06
      if(iloop.eq.1) diap=10.d-09
      write(6,1005) iloop, diap
1005  format(/,' iloop, diap ',i5,e12.5)
c
      call attenk(tkcomp,tdcomp,rhop,rhof,anuf,alphap,diap,
     1            ektpsu)
c
800   continue
      stop
```

```
      end

      subroutine attenk(tkcomp,tdcomp,rhop,rhof,anuf,alphap,diap,
     1            ektpsu)
c     Computes attenuation of turbulent kinetic energy due to small
c     particles entrained by a fluid. Adapted from: A. M. Al Taweel,
c     J. Landau, Turbulence modulation in two-phase jets. Int. J.
c     Multiphase Flow, 3 (1977), pp. 341-351.
c
c     INPUT:
c     tdcomp = dissipation of turbulent kinetic energy computed from
c              a driver program;
c     tkcomp = turbulent kinetic energy computed from a driver pro-
c              ogram without taking into accout attenuation;
c     alphap, diap, anuf, rhof, rhop;
c
c     OUTPUT: ektpsu= attenuated value of turbulent kinetic energy.
c
      implicit real*8 (a-h, o-z)
      common/ektp/ adash,vel
c
      data iwrite,imax,i1,ngauss/0,300,80,6/
      vel=100.d0
      vel=2.d0
      alphaf=1.d0-alphap
      eta=(anuf**3/tdcomp)**0.25d0
      al=eta*1.d04
      akamin=1.d0/al
      akaint=30.d0
      akamax=1.d04
      ddk=akamax-akamin
      gsi=1.5d0
      ww=alphap*rhop/(alphap*rhop + alphaf*rhof)
      phi=rhop/rhof
      chi=0.5d0
      oned3=1.d0/3.d0
      twod3=2.d0/3.d0
      fived3=5.d0/3.d0
c
      if(iwrite.eq.0) then
      write(6,997)
      write(6,999) imax,i1, al,  akamin,akaint,akamax
      write(6,998) alphap, ww, vel, tdcomp
997   format(/,' INFORMATION FROM SUBROUTINE ATTENK',/)
998   format(' alphap, loading=ww, vel, tdcomp', 4e12.5,/)
999   format('  imax,i1,al,akamin/int/max ',2i4, 4e11.5)
      iwrite=1
      endif
c
      delta1=(akaint - akamin)/float(i1)
      delta2=(akamax-akaint)/float(imax-i1)
      adash=18.d0*anuf/(diap**2*(phi+chi))
c
      eksu=0.d0
      ektpsu=0.d0
```

```
      sumddk=0.d0
      do 500 i=1,imax
      ii=i-i1
      if(i.le.i1) ak= akamin +(i-1)*delta1 + delta1/2.d0
      if(i.gt.i1) ak= akaint +(ii-1)*delta2 + delta2/2.d0
      if(i.le.i1) sumddk=sumddk + delta1
      if(i.gt.i1) sumddk=sumddk + delta2
c
c     Integrate in two intervals if upper integration limit ak > akaint.
      if(ak.lt.akaint) then
      call gaussi(akamin,ak,ngauss,aik)
      else
      call gaussi(akamin,akaint,ngauss,aik1)
      call gaussi(akaint,ak, ngauss,aik2)
      aik=aik1 + aik2
      endif
c
      power=36.d0*ww*gsi*anuf*tdcomp**(-oned3)*aik/(phi*diap**2)
      ek   =twod3*tkcomp*ak**(-fived3)/
     1        (akamin**(-twod3) - akamax**(-twod3))
      hk=exp(-power)
      ektp=ek*hk
c
c     if(i.eq.imax) write(6,1000) i, aik1, aik2, aik
1000  format(' i, aik1,aik2,aik ',i5,3e12.5)
c     if(i.eq.imax) write(6,2000) i, ak,hk, ek, ektp
2000  format(' i,ak,hk,ek,ektp ',i4,4e11.4)
c
      if(i.le.i1) then
      eksu=   eksu +   ek   *delta1
      ektpsu= ektpsu + ektp *delta1
      else
      eksu=   eksu +   ek   *delta2
      ektpsu= ektpsu + ektp *delta2
      endif
500   continue
c
c     Compute the percentual deviation between the input value of the
c     turbulent kinetic energy (tkcomp) and the value (eksu) obtained
c     by integrating the spectral distribution.
      error=abs(tkcomp-eksu)/tkcomp
      hkmean= ektpsu/eksu
      write(6,1001) tkcomp, eksu, ektpsu, hkmean, error
      write(6,1009) ddk,sumddk
1001  format(' tkcomp,eksu/tpsu,hkmean,error ',5e12.5)
1009  format(' ddk,sumddk ',2e12.5)
c
      return
      end



      subroutine gaussi(a,b,n,sum)
c-----------------------------------------------------------------------
c     computes a definite integral with gaussian quadrature
```

```
c      input= a,b limits of integration (finite)
c             n= order of gaussian quadrature
c             r,w= arrays containing zeros and weigths of Legendre
c                  polynoms
c             anteg (external) function to be integrated
c      output= sum= computed integral
c
       implicit real*8 (a-h, o-z)
       dimension r(50),w(50)
c
c      introduce constants
       if(n.eq.6) go to 60
       if(n.eq.10) go to 100
       if(n.eq.12) go to 120
       if(n.eq.20) go to 200
       if(n.eq.40) go to 400
60     continue
       r(4)=0.23861918608319690863d0
       r(5)=0.66120938646626451366d0
       r(6)=0.93246951420315202781d0
       r(3)=-r(4)
       r(2)=-r(5)
       r(1)=-r(6)
c
       w(4)=0.46791393457269104739d0
       w(5)=0.36076157304813860757d0
       w(6)=0.17132449237917034504d0
       w(3)=w(4)
       w(2)=w(5)
       w(1)=w(6)
       go to 500
100    continue
       r(6)=0.14887 43389 81631 21089d0
       r(7)=0.43339 53941 29247 19080d0
       r(8)=0.67940 95682 99024 40623d0
       r(9)=0.86506 33666 88984 51073d0
       r(10)=0.97390 65285 17171 72008d0
c
       w(6)=0.29552 42247 14752 87017d0
       w(7)=0.26926 67193 09996 35509d0
       w(8)=0.21908 63625 15982 04400d0
       w(9)=0.14945 13491 50580 59315d0
       w(10)=0.06667 13443 08688 13759d0
c
       do 105 i=1,5
       k=11-i
       r(i)=-r(k)
105    w(i)=w(k)
       go to 500
120    continue
       r(7)=0.12523 34085 11468 91547d0
       r(8)=0.36783 14989 98180 19375d0
       r(9)=0.58731 79542 86617 44730d0
       r(10)=0.76990 26741 94304 68704d0
       r(11)=0.90411 72563 70474 85668d0
```

```
      r(12)=0.98156 06342 46719 25069d0
c
      w(7)=0.24914 70458 13402 78500d0
      w(8)=0.23349 25365 38354 80876d0
      w(9)=0.20316 74267 23065 92175d0
      w(10)=0.16007 83285 43346 22633d0
      w(11)=0.10693 93259 95318 43096d0
      w(12)=0.04717 53363 86511 82719d0
c
      do 125 i=1,6
      k=13-i
      r(i)=-r(k)
125   w(i)=w(k)
      go to 500
c
200   continue
      r(20)=0.9931285991850949247 9d0
      r(19)=0.9639719272779137912 7d0
      r(18)=0.9122344282513259058 7d0
      r(17)=0.8391169718222188233 9d0
      r(16)=0.7463319064601507926 1d0
      r(15)=0.6360536807265150254 5d0
      r(14)=0.5108670019508270980 0d0
      r(13)=0.3737060887154195606 7d0
      r(12)=0.2277858511416450780 8d0
      r(11)=0.0765265211334973337 5d0
c
      w(20)=0.0176140071391521183 1d0
      w(19)=0.0406014298003869413 3d0
      w(18)=0.0626720483341090635 7d0
      w(17)=0.0832767415767047487 3d0
      w(16)=0.1019301198172404350 4d0
      w(15)=0.1181945319615184173 1d0
      w(14)=0.1316886384491766269 0d0
      w(13)=0.1420961093183820513 3d0
      w(12)=0.1491729864726037467 9d0
      w(11)=0.1527533871307258507 0d0
c
      do 205 i=1,10
      k=21-i
      r(i)=-r(k)
205   w(i)=w(k)
      go to 500
c
400   continue
c
      r(40)=0.9982377097105592003 5d0
      r(39)=0.9907262386994570064 5d0
      r(38)=0.9772599499837742626 6d0
      r(37)=0.9579168192137916558 0d0
      r(36)=0.9328128082786765333 6d0
      r(35)=0.9020988069688742967 3d0
      r(34)=0.8659595032122595038 2d0
      r(33)=0.8246122308333116632 0d0
      r(32)=0.7783056514265193876 9d0
```

```
      r(31)=0.727318255189927103 28d0
      r(30)=0.671956684614179548 38d0
      r(29)=0.612553889667980237 95d0
      r(28)=0.549467125095128202 08d0
      r(27)=0.483075801686178712 91d0
      r(26)=0.413779204371605001 52d0
      r(25)=0.341994090825758473 01d0
      r(24)=0.268152185007253681 14d0
      r(23)=0.192697580701371099 72d0
      r(22)=0.116084070675255208 48d0
      r(21)=0.038772417506050821 93d0
c
      w(40)=0.004521277098533191 26d0
      w(39)=0.010498284531152813 62d0
      w(38)=0.016421058381907888 71d0
      w(37)=0.022245849194166957 26d0
      w(36)=0.027937006980023401 10d0
      w(35)=0.033460195282547847 39d0
      w(34)=0.038782167974472017 64d0
      w(33)=0.043870908185673271 99d0
      w(32)=0.048695807635072232 06d0
      w(31)=0.053227846983936824 36d0
      w(30)=0.057439769099391551 37d0
      w(29)=0.061306242492928939 17d0
      w(28)=0.064804013456601038 07d0
      w(27)=0.067912045815233903 83d0
      w(26)=0.070611647391286779 70d0
      w(25)=0.072886582395804059 06d0
      w(24)=0.074723169057968264 20d0
      w(23)=0.076110361900626242 37d0
      w(22)=0.077039818164247965 59d0
      w(21)=0.077505947978424811 26d0
      do 405 i=1,20
      k=41-i
      r(i)=-r(k)
405   w(i)=w(k)
500   continue
c
c     change the variable so that the integration limits range from (-1,+1).
c     this is equivalent to shift the zeros
c
      do 510 i=1,n
510   r(i)=(r(i)*(b-a)+a+b)/2.d0
c
c     compute the function to be integrated in the shifted zeros
c     and multiply by respective weights
c
      sum=0.d0
c
      do 541 i=1,n
      bet=anteg(r(i))
      sum=sum+bet*w(i)
541   continue
c
c     multiply by (b-a)/2. (because of the change of dx)
```

```
c
900   continue
      sum=sum*(b-a)/2.d0
c
      return
      end

      function anteg(r)
      implicit real*8 (a-h, o-z)
      common/ektp/ adash,vel
      adash2=adash**2
      costh=1.d0/dsqrt(1.d0 + (vel*r/adash)**2)
      ada= adash2/(((vel*r)**2 + adash2) * costh)
      rk=sqrt(1.d0 + ada**2 -2.d0*ada*costh)
      anteg=rk**2/r**(5.d0/3.d0)
      return
      end
```

Sample OUTPUT from Program PARTVI

```
iloop, diap     1  .10000E-07

INFORMATION FROM SUBROUTINE ATTENK

 imax,il,al,akamin/int/max  300   80 .14026E+01 .71298E+00 .30000E+02 .10000E+05
alphap, loading=ww, vel, tdcomp  .50000E-02  .80723E+00  .20000E+01  .10000E+02

tkcomp,eksu/tpsu,hkmean,error   .20000E+00  .19651E+00  .19651E+00  .10000E+01  .17454E-01
ddk,sumddk   .99993E+04  .99993E+04

iloop, diap     2  .10000E-03
tkcomp,eksu/tpsu,hkmean,error   .20000E+00  .19651E+00  .13038E+00  .66350E+00  .17454E-01
ddk,sumddk   .99993E+04  .99993E+04

iloop, diap     3  .20000E-03
tkcomp,eksu/tpsu,hkmean,error   .20000E+00  .19651E+00  .93489E-01  .47575E+00  .17454E-01
ddk,sumddk   .99993E+04  .99993E+04

iloop, diap     4  .30000E-03
tkcomp,eksu/tpsu,hkmean,error   .20000E+00  .19651E+00  .76465E-01  .38912E+00  .17454E-01
ddk,sumddk   .99993E+04  .99993E+04

iloop, diap     5  .40000E-03
tkcomp,eksu/tpsu,hkmean,error   .20000E+00  .19651E+00  .73873E-01  .37592E+00  .17454E-01
ddk,sumddk   .99993E+04  .99993E+04

iloop, diap     6  .50000E-03
tkcomp,eksu/tpsu,hkmean,error   .20000E+00  .19651E+00  .81353E-01  .41399E+00. .17454E-01
ddk,sumddk   .99993E+04  .99993E+04

iloop, diap     7  .60000E-03
tkcomp,eksu/tpsu,hkmean,error   .20000E+00  .19651E+00  .94041E-01  .47856E+00  .17454E-01
ddk,sumddk   .99993E+04  .99993E+04

iloop, diap     8  .70000E-03
tkcomp,eksu/tpsu,hkmean,error   .20000E+00  .19651E+00  .10793E+00  .54922E+00  .17454E-01
ddk,sumddk   .99993E+04  .99993E+04

iloop, diap     9  .80000E-03
tkcomp,eksu/tpsu,hkmean,error   .20000E+00  .19651E+00  .12082E+00  .61486E+00  .17454E-01
ddk,sumddk   .99993E+04  .99993E+04

iloop, diap    10  .90000E-03
tkcomp,eksu/tpsu,hkmean,error   .20000E+00  .19651E+00  .13196E+00  .67153E+00  .17454E-01
ddk,sumddk   .99993E+04  .99993E+04

iloop, diap    11  .10000E-02
tkcomp,eksu/tpsu,hkmean,error   .20000E+00  .19651E+00  .14127E+00  .71891E+00  .17454E-01
ddk,sumddk   .99993E+04  .99993E+04

iloop, diap    12  .11000E-02
tkcomp,eksu/tpsu,hkmean,error   .20000E+00  .19651E+00  .14896E+00  .75805E+00  .17454E-01
```

```
ddk,sumddk    .99993E+04   .99993E+04

iloop, diap     13  .12000E-02
tkcomp,eksu/tpsu,hkmean,error    .20000E+00  .19651E+00  .15530E+00  .79031E+00  .17454E-01
ddk,sumddk    .99993E+04   .99993E+04

iloop, diap     14  .13000E-02
tkcomp,eksu/tpsu,hkmean,error    .20000E+00  .19651E+00  .16055E+00  .81700E+00  .17454E-01
ddk,sumddk    .99993E+04   .99993E+04

iloop, diap     15  .14000E-02
tkcomp,eksu/tpsu,hkmean,error    .20000E+00  .19651E+00  .16491E+00  .83918E+00  .17454E-01
ddk,sumddk    .99993E+04   .99993E+04

iloop, diap     16  .15000E-02
tkcomp,eksu/tpsu,hkmean,error    .20000E+00  .19651E+00  .16856E+00  .85775E+00  .17454E-01
ddk,sumddk    .99993E+04   .99993E+04

iloop, diap     17  .16000E-02
tkcomp,eksu/tpsu,hkmean,error    .20000E+00  .19651E+00  .17163E+00  .87341E+00  .17454E-01
ddk,sumddk    .99993E+04   .99993E+04

iloop, diap     18  .17000E-02
tkcomp,eksu/tpsu,hkmean,error    .20000E+00  .19651E+00  .17425E+00  .88670E+00  .17454E-01
ddk,sumddk    .99993E+04   .99993E+04

iloop, diap     19  .18000E-02
tkcomp,eksu/tpsu,hkmean,error    .20000E+00  .19651E+00  .17648E+00  .89807E+00  .17454E-01
ddk,sumddk    .99993E+04   .99993E+04

iloop, diap     20  .19000E-02
tkcomp,eksu/tpsu,hkmean,error    .20000E+00  .19651E+00  .17840E+00  .90785E+00  .17454E-01
ddk,sumddk    .99993E+04   .99993E+04

iloop, diap     21  .20000E-02
tkcomp,eksu/tpsu,hkmean,error    .20000E+00  .19651E+00  .18006E+00  .91631E+00  .17454E-01
ddk,sumddk    .99993E+04   .99993E+04

iloop, diap     22  .21000E-02
tkcomp,eksu/tpsu,hkmean,error    .20000E+00  .19651E+00  .18151E+00  .92369E+00  .17454E-01
ddk,sumddk    .99993E+04   .99993E+04

iloop, diap     23  .22000E-02
tkcomp,eksu/tpsu,hkmean,error    .20000E+00  .19651E+00  .18278E+00  .93014E+00  .17454E-01
ddk,sumddk    .99993E+04   .99993E+04

iloop, diap     24  .23000E-02
tkcomp,eksu/tpsu,hkmean,error    .20000E+00  .19651E+00  .18390E+00  .93583E+00  .17454E-01
ddk,sumddk    .99993E+04   .99993E+04

iloop, diap     25  .24000E-02
tkcomp,eksu/tpsu,hkmean,error    .20000E+00  .19651E+00  .18489E+00  .94086E+00  .17454E-01
ddk,sumddk    .99993E+04   .99993E+04

iloop, diap     26  .25000E-02
tkcomp,eksu/tpsu,hkmean,error    .20000E+00  .19651E+00  .18576E+00  .94532E+00  .17454E-01
ddk,sumddk    .99993E+04   .99993E+04
```

```
iloop, diap    27  .26000E-02
tkcomp,eksu/tpsu,hkmean,error   .20000E+00  .19651E+00  .18655E+00  .94931E+00  .17454E-01
ddk,sumddk   .99993E+04  .99993E+04

iloop, diap    28  .27000E-02
tkcomp,eksu/tpsu,hkmean,error   .20000E+00  .19651E+00  .18725E+00  .95288E+00  .17454E-01
ddk,sumddk   .99993E+04  .99993E+04

iloop, diap    29  .28000E-02
tkcomp,eksu/tpsu,hkmean,error   .20000E+00  .19651E+00  .18788E+00  .95609E+00  .17454E-01
ddk,sumddk   .99993E+04  .99993E+04

iloop, diap    30  .29000E-02
tkcomp,eksu/tpsu,hkmean,error   .20000E+00  .19651E+00  .18845E+00  .95898E+00  .17454E-01
ddk,sumddk   .99993E+04  .99993E+04
```

Distribution for ANL-95/6

Internal:

M. Bottoni (5)
J. X. Bouillard
J. F. C. Chang
T. H. Chien
H. M. Domanus
H. Drucker
R. W. Lyczkowski
C. A. Malefyt
R. B. Poeppel
W. T. Sha (5)
J. G. Sun
R. A. Valentin
R. W. Weeks
TIS Files

External:

DOE-OSTI for distribution per UC-113 (52)
ANL Libraries
ANL-E (2)
ANL-W
Manager, Chicago Field Office, DOE
Energy Technology Division Review Committee:
H. K. Birnbaum, University of Illinois, Urbana
R. C. Buchanan, University of Cincinnati, Cincinnati, OH
M. S. Dresselhaus, Massachusetts Institute of Technology, Cambridge, MA
B. G. Jones, University of Illinois, Urbana
C.-Y. Li, Cornell University, Ithaca, NY
S. N. Liu, Fremont, CA
R. E. Smith, SciTech, Inc., Morrisville, NC
W. Sengpiel, KfK, Germany